Accepted Manuscript

Geological Society, London, Special Publications

Variations in Aridity across the Asia-Australia Region during the Neogene and their Impact on Vegetation

Peter D. Clift

DOI: https://doi.org/10.1144/SP549-2023-58

To access the most recent version of this article, please click the DOI URL in the line above. When citing this article please include the above DOI.

Received 21 March 2023
Revised 6 July 2023
Accepted 13 July 2023

Variations in Aridity across the Asia-Australia Region during the Neogene and their Impact on Vegetation

Peter D. Clift[1,2*] (ORCID 0000-0001-6660-6388)

1 - Department of Earth Sciences, University College London, London WC1E 6BS, UK

2 - Department of Geology and Geophysics, Louisiana State University, Baton Rouge, LA 70803, USA

* Correspondence (peter.clift@ucl.ac.uk)

Abstract

Scientific drilling provides extended records of continental environmental conditions during the Neogene in Asia and northern Australia. Spectral data allows reconstruction of the environment using abundances of hematite and goethite. Hematite formation is favoured by dry or seasonal conditions. Hemipelagic sites show the most regular records. Monsoon strengthening started in the Early Miocene and peaked at 17–20 Ma in the Bay of Bengal and at 10–15 Ma in southern China before weakening after ~12 Ma and ~10 Ma respectively. The Indus dried after ~8 Ma and again after 3 Ma, while eolian sediment sources to the Sea of Japan show increased aridity after 5 Ma and 3 Ma. The Mekong indicates increasing aridity after 6 Ma, similar to Eastern Australia. In contrast, NW Australia shows a trend towards wetter conditions after 8 Ma, a humid period at 4–6 Ma, followed by drying. There is a link between drying and vegetation in the Mekong and Pearl River basins, as well as Eastern Australia. Monsoon strengthening is linked to topographic uplift in the Himalaya, together with Tethyan gateway closure. Long term drying is likely driven by global cooling since the Middle Miocene.

Keywords: Monsoon, aridity, diffuse reflectance spectroscopy, International Ocean Discovery Program

The climate of Asia is presently dominated by the monsoon system, which affects the southern and eastern parts of the continent, with summer rain reaching far into the continent interior (Wang 2006). The Asian monsoon is largely driven by the temperature contrast between the continents and oceans (Webster 1987), although it is increasingly recognized that topography plays a key role in guiding where the moisture evaporated from the ocean is directed, prior to final precipitation (Acosta & Huber 2020; Kutzbach et al. 1993). Modelling has emphasised the role of uplift of the Himalayan barrier and Tibetan Plateau (Boos & Kuang 2010; Farnsworth et al. 2019; Kutzbach et al. 1993) especially to the South Asian Monsoon, although in this region the influence of orbital precession, atmospheric CO_2 concentrations, ice-sheet extent, and ocean gateways was also recognized (Thomson et al. 2021). Most recently the effects of topographic uplift in East Africa and the Iranian Plateau have also been identified as being influential in steering moisture into the continental interior in South Asia (Sarr et al. 2022). The distribution of moisture has necessarily been a critical control over the biosphere across Asia, both in terms of total precipitation, and in seasonality (Ehlers et al. 2022).

As a result of these conceptual advances in what drives the monsoon, the idea that the monsoon has behaved in a homogenous fashion across the continent over long periods of geologic time seems increasingly unlikely. Unfortunately, testing of models has been limited by a shortage of detailed climatic and environmental reconstructions. There have been numerous disagreements about fundamental trends, with competing groups advancing opposing models, e.g., favouring either weakening or strengthening of the monsoon during the Late Miocene (Betzler et al. 2016; Clift et al. 2014; Feakins et al. 2020; Kroon et al. 1991). Some of the apparent disagreement stems from whether researchers are using wind or rainfall-based proxies that are not always coupled. In this work constraining rainfall and humidity is the primary objective. Reconstructing palaeo-monsoon intensity has been problematic, because of difficulties in identifying appropriate proxies and because continuous, well-dated sedimentary sections that might record monsoon have often been lacking.

The latter problem has been partly addressed as a result of a campaign of scientific drilling by International Ocean Discovery Program (IODP) that was completed in the late 2010's and spanned the region between the Arabian Sea and the Sea of Japan (Fig. 1). Drilling was also undertaken around NW Australia and provided a significant improvement in the duration of the sedimentary record that can be studied in order to constrain monsoon intensity (Clift et al. 2022). In this study, I compile sedimentary sections from across the Indian Ocean, SE Asia, and northern Australian regions to see how continental environments have evolved through time. The goal is to see whether environmental change occurred synchronously across Asia and even Australia during

the Neogene, and whether the direction of change (i.e., wetter or drier) was also the same in these contrasting regions. I further use organic geochemistry and pollen data to see whether these changes could have impacted the nature of vegetation.

Continental environmental conditions can be constrained using spectral colour analysis (diffuse reflectance spectroscopy (DRS))(Kortüm et al. 1963), which reflects the mineralogy of the sediments in the core. In turn these are products of the environmental and chemical weathering conditions in the source regions that favour formation of certain critical minerals. The emphasis of this study is on the aridity of the continental interior, both the amount of rainfall delivered to each drainage system, as well as the seasonality. It should be remembered that continental rainfall differs from oceanic productivity and need not vary at the same time or in the same direction, even if they are driven by the same wind systems. It is well accepted that the strength of upwelling and productivity in the Arabian Sea is largely influenced by the summer wind strength (Curry et al. 1992), whereas the precipitation onshore is more complicated, and while linked to wind, is also controlled by the strength of the hydrological cycle in the atmosphere, which is in turn related to global temperature (Trenberth et al. 2007). Other important factors include the location of the Westerly Jet, and regional topography, which steers moisture into the continental interior (Acosta & Huber 2017; Sarr et al. 2022). Moreover, global climate change, in the form of progressive cooling during the Neogene has largely acted to reduce the amount of moisture in the atmosphere (Caves Rugenstein & Chamberlain 2018; Miao et al. 2012) so that stronger winds, driving more powerful upwelling do not necessarily result in heavier rainfall.

In this work, DRS data that was collected during drilling cruises of the Ocean Drilling Program (ODP), Integrated Ocean Drilling Program (IODP) and International Ocean Discovery Program (IODP) have been compiled. These data were mostly collected at sea on freshly cut core using spectral cameras, initially handheld during ODP and then later by automated cameras during IODP. The cameras provide exceptionally high-resolution, low-cost analysis beyond what would be possible by conventional mineral or chemical analysis and allow centimetre-scale changes to be recorded in sedimentary sections that span hundreds of metres or even more than 1 km length.

The focus of this study is on colour spectral characteristics that represent increased drying or stronger seasonality in the core. Although the monsoon is associated with summer rains, it is also characterised by strong seasonality and the occurrence of a distinct dry season. This approach has been used on several occasions in the past and allows relatively subtle changes in the abundance of environmentally sensitive minerals to be identified. For example, the proportion of hematite in a core might be very low, especially when accumulated in a distal hemipelagic setting, but the effect

on the colour of the core can, nonetheless, be quite significant. Considering the low content of hematite and goethite in deep sea sediment, usually less than 1%, it is difficult to measure their contents via more conventional methods, for example XRD (Deaton & Balsam 1991; Zhang et al. 2007). However, a spectral camera can identify relatively minor changes that would not be possible through bulk sediment analysis.

The usefulness of the spectral method for monsoon studies has been demonstrated by earlier studies in the South China Sea. Clift *et al*. (2014) showed that peak hematite/goethite values (Fig. 2E) correlate well with high values of $^{87}Sr/^{86}Sr$ isotopes (Fig. 2D), which are linked to strong chemical weathering as well as provenance (France-Lanord et al. 1993). They also correlate with the pollen assemblages of central Asia that show high degrees of humidity in the Middle Miocene (Fig. 2F), suggesting a link between high hematite/goethite values and strong monsoon rainfall and seasonality. This was also a time when clay mineral assemblages, particularly in the form of high smectite/kaolinite values (Fig. 2A), indicated a seasonal rather than a tropical climate. In general, there was a poor correlation between hematite/goethite values and chemical weathering proxies such as the Chemical Index of Alteration or K/Al (Nesbitt et al. 1980). This implies a general decoupling of chemical weathering with monsoon rainfall intensity. Although on long timescales fast sedimentation rates in marginal seas are related to times of stronger monsoon and high hematite/goethite values (Clift 2006) it is not apparent that at a single drilling site, whether there is a close correlation between mass flux to the ocean proxied by Ti/Ca (Fig. 2C) and hematite/goethite values. Magnetic susceptibility, which has been used as a climatic proxy in the Chinese Loess Plateau (An et al. 1991) shows a closer association to Ti/Ca here and implies that it may be a proxy for clastic flux rather than weathering state or environment. Although provenance could play a part in controlling hematite/goethite values, in the case of the northern South China Sea, this can be eliminated this possibility because provenance is known to be relatively straightforward and entirely sourced within the South China block (Liu et al. 2022).

In this study the idea that the Asian monsoon experienced a significant change in its intensity ~7–8 Ma is tested using spectral analysis, and I further investigate if changes at that time in Asia were paralleled by changes in the monsoon in Northern Australia. In the modern oceans the monsoon in Southeast Asia represents a parallel system to that affecting Queensland and northeast Australia, as a result of the Intertropical Convergence Zone (ITCZ), moving across the equator on a seasonal basis (Berry & Reeder 2014).

Data Coverage

In order to compare climatic evolution across Asia and Australia several scientific drilling data sets, many acquired within the last ten years, were integrated. Records for the Arabian Sea are taken from IODP Site U1456, located on the east side of the Indus Fan in the Laxmi Basin, and recovered by IODP Expedition 355 (Pandey et al. 2016)(Fig. 1). Although the pre-10 Ma record is lost because of mass wasting from the Indian margin (Calvès et al. 2015), the drilling provides a mostly continuous record of weathering and erosion in the Indus Basin since that time (Routledge et al. 2020). There was monsoon-related drilling in the Maldives during Expedition 359 (Betzler et al. 2017), but this area is not considered in this study because it only addressed biogenic production and would not provide any constraints about environmental conditions onshore. IODP Site U1451 drilled during Expedition 354 in the central Bay of Bengal (France-Lanord et al. 2015) is selected because it is the longest continuous section reflecting conditions in the central and eastern Himalaya and associated flood plains. This record spans more than 20 m.y. and has a constant provenance (Ali et al. 2021), although there are short breaks related to the avulsion of submarine fan lobes. ODP Site 718 was drilled during Leg 116 at the distal southern end of the Bengal Fan where the recovered section spans ~17 m.y. (Shipboard Scientific Party 1989), again with a constant Himalayan source (Bouquillon et al. 1990).

Another record from the Bay of Bengal comes from IODP Site U1443, drilled during Expedition 353 on the 90 East Ridge (Fig. 1). Because of this position on the ridge, the section mostly comprises hemipelagic, biogenic and eolian sediments, which were supplied largely from the Bengal delta and Indo-Burman ranges, but potentially with lesser amounts eroded from peninsular India and the Irrawaddy (Ayeyarwady) River (Bretschneider et al. 2021). The sequence is much more condensed than the other sites in the Indian Ocean, but consequently it spans a particularly long time period, ~29 m.y. (Clemens et al. 2016). The submarine fan on the east side of 90 East Ridge is known as the Nicobar Fan but is interpreted to be a part of the wider Bengal Fan (McNeill et al. 2017a). Data from IODP Site U1480 drilled during Expedition 362 provides 20 m.y. of clastic sedimentary record, although only 10 m.y. is considered to be associated with discharge from the Bengal Delta (McNeill et al. 2017b). IODP Site U1433, cored during Expedition 349 in the SW South China Sea (Li et al. 2015), is believed to have derived its sediment from the Mekong River since ~8.5 Ma, but had a more local provenance before that time that likely was not similar to the upper reaches of the Mekong where sediment is now derived (Liu et al. 2017). Consequently, the pre-8.5 Ma provenance is not considered in the environmental reconstruction. ODP Site 1148 was cored during ODP Leg 184 (Wang et al. 2000b) and contains at least 24 m.y. of weathering records from southern China, likely from the Pearl River (Clift et al. 2002). The site has long been recognized as a continuous hemipelagic record of the monsoon in southern China. The top of the section at Site

1148 is affected by mass wasting (Shipboard Scientific Party 2000) and so the record from ODP Site 1146, located slightly to the east and which has a 20 m.y. record with no known disruption at the top (Wang et al. 2000a) was also used.

In the Sea of Japan, located at the far northeast corner of the monsoon zone, IODP Expedition 346 drilled at Site U1430 where sediment was dominantly supplied by eolian sedimentation, with lesser degrees of hemipelagic sedimentation originating from Japan (Tada et al. 2015). The record here spans >12 m.y., albeit with a hiatus at 5–7 Ma. Finally, two sites from the Australian margin were examined. IODP Site U1464 is from NW Australia and was drilled during IODP Expedition 356. Unfortunately, spectral data are not available at this site but basic colour data can be examined. The sequence is dated to record ~13.5 m.y. of run-off from the adjacent continent (Gallagher et al. 2017). An older drilling site, ODP Site 1195, recovered during ODP Leg 194 from eastern Australia records 18.4 m.y. of erosion and weathering in central Queensland (Isern et al. 2002). In all cases I use the shipboard age assignments to calculate depositional ages, unless they have been subsequently revised, e.g., at IODP Site U1464 (Groeneveld et al. 2017). Microfossil and magnetic age picks were converted to a numerical age using the time scale of Gradstein *et al.* (2020). Taken together these cores represent a wide survey across the Indian Ocean and Asia-Pacific region and are chosen to provide reconstructions of evolving environments in this area during the Neogene. In all cases the spectral files were downloaded from the IODP databank either using the LIMS system (https://web.iodp.tamu.edu/LORE/) for IODP wells or Janus (http://www-odp.tamu.edu/database/janusmodel.htm) for ODP. The data is 100% open access.

Methods

Environmental conditions are an important control over chemical weathering. In turn they affect the chemistry and mineralogy of sediments carried from any given continental source to the ocean, whether transported by water or wind. The sediment composition also reflects source rock compositions, but if provenance can be constrained then changes in sediment character can be used to reconstruct the evolution of environmental conditions within a drainage basin. The well constrained hematite/goethite proxy was employed where possible. This is derived from spectral reflectance measurements, which has already been used to interpret palaeoenvironmental conditions through time in both SE Asia and southern China, as well as the Atlantic Ocean (Balsam & Damuth 2000; Clift 2006; Giosan et al. 2002; Hu et al. 2012; Ji et al. 2002). Because iron is common component of rocks it is not thought be sensitive to provenance. The presence of Fe-oxides in the sediment can be constrained by colour, as well the first derivative of the reflectance spectrum (Deaton & Balsam 1991; Kosmas et al. 1986).

Hematite usually forms in drier, warmer environments (Schwertmann 1971), while goethite is generally associated with cooler, wetter environments (Sangode & Bloemendal 2004; Schwertmann 1971). The ratio of the two has previously been used as a proxy of relative humidity (Balsam et al. 1997; Giosan et al. 2002). This proxy may be subject to change during diagenesis. Iron oxide reduction, which can affect the measured ratio is typically limited to the upper 1 m of the sediment column (Canfield et al. 1992), but would not be significant on the scale considered here, i.e., several hundred meters of subseafloor penetration. Rapidly deposited Fe-rich sediments with modest organic carbon contents retain some of the original iron oxides through the shallow reduction zone (Roberts 2015). This effect may however affect the more slowly accumulating sediments on the 90 East Ridge and even Sea of Japan, but not the rapidly accumulating sediment in the submarine fans in other settings.

Spectral reflectance data were collected from ODP sediment cores using a hand-held Minolta CM-2002 Spectrophotometer. This work was done as soon as the core was split after recovery. During IODP expeditions spectral data are derived from the Section Half Multisensor Logger (SHMSL), which is an automated system. Unfortunately, many of the IODP SHMSL data are considered to be unreliable at short wavelengths (<500 nm) because the light source employed at the time of the monsoon expeditions had little power at those values. This resulted in a failure to capture the first-derivative peak at 435 nm, which is associated with goethite, although longer wavelengths and proxies such as a* (redness) and b* (blueness) were considered reliable (Liu et al. 2019). The cores from IODP Sites U1456 and U1433 have however been re-measured using a Minolta CM-2002 Spectrophotometer, which has a proven track record, although the scanning had to be done on older cores that have experienced some oxidation (Liu et al. 2017; Zhou et al. 2021). I use the 565 nm first derivative as an indicator of hematite content alone, although there are issues related to the matrix in which the mineral is held. If the matrix is constant, then the height of the peak can be used as a proxy for abundance (Deaton & Balsam 1991), but since this is not always the case between different drill sites, this particular proxy needs to be interpreted with caution.

Results

Because of the data quality issues related to the 435 nm data, I first examine how the DRS and colour proxies compare with one another in order to establish the most reliable for constraining aridity in the continental interior. Figure 3A shows the relationship between 565 nm intensity (hematite), and the a* proxy. These data represent 10 point running averages for each of the sites because the full data sets can be noisy and the emphasis here is on long-term trends, not short excursions. There is a good correlation between a* and 565 nm, suggesting that the concentration of

hematite in the core is an important control on its redness. This is a relationship which is common across the entire dataset. In contrast Figure 3B shows the relationship between a* and b* which is a proxy for the blueness of the sediment. This does not show a close relationship, as might be expected, but only highlights the fact that sediments from eastern Australia and from the oldest part of the section at Site U1433 (Mekong) are bluer than other sediments, while those from U1464 (NW Australia), Site U1430 (Sea of Japan) and Site U1443 (90 East Ridge) are the most yellow. The plot also highlights that Site U1443 (90 East Ridge) has the reddest sediment.

Likewise, the goethite-sensitive 435 nm proxy can be compared to the a* and b* proxies that are routinely collected in a reliable fashion even when 435 nm data is not available. Figure 4A shows that there is essentially no correlation between the goethite abundance and the a* proxy, with all of the data forming a homogenous cluster. Figure 4B however, shows that there is some relationship between the b* and goethite abundance. There is a good deal of scatter in this relationship as well, although in general sediments which are more blue in colour seem to have more goethite. This is particularly true for the material from Site 1195 in eastern Australia but is less applicable to the Mekong and Bay of Bengal, Sites U1433 and 718 respectively.

Evolution since 25 Ma

The temporal evolution in these DRS properties is now considered in order to assess the long-term variability in climate across the area since 25 Ma. As well as the smoothed data plotted for each site, I also provide a simplified depiction of the range in values as a coloured log to highlight large scale changes. Figure 5 shows how variations in 565/435 values compare across the region. Site U1456 (Indus Fan) has high values that peak at ~3 Ma, following a gradual rise since 10 Ma and followed by a decrease since 1 Ma. Provenance studies indicate more erosion from the Himalaya and from Peninsular India, and less from the Karakoram since 3 Ma (Cai et al. 2019; Clift et al. 2019). This may impact the most recent trend, although weathering is still inferred to have dominantly occurred on the Indus flood plains throughout and should not be heavily provenance affected. Site U1451 (Bengal Fan) shows a noisy, random scatter, even after smoothing, confirming the poor quality of the 435 nm data. These are not useful proxy data at this site. The distal Site 718 (Bengal Fan) shows little long-term trend, but generally has lower 565/435 values than Site U1456 (Indus Fan). There are short lived peaks and troughs, most notably at 16–17 Ma and 11–12 Ma at Site 718. Site U1433 (Mekong) has lower 565/435 values than much of the sediment in the Indian Ocean submarine fans. Since the establishment of the Mekong at its present location (~8.5 Ma) 565/435 values have shown a long-term rise, especially after 6 Ma and 2 Ma. Both Pearl River sites (1146 and 1148) have similar overall forms and have the greatest range of values, but with relatively low variability at any given

time. 565/435 values are very low at 15–17 Ma then reach a maximum from 15 to 10 Ma, declining to ~5 Ma and remained low since that time. Site 1148 has higher 565/435 values than sediments from Site 1146 and this reflects greater dilution of the hematite signal in the presence of greater biogenic carbonate concentrations at Site 1146 (Wang et al. 2000a). Finally, Site 1195 (East Australia) shows low variability and low values, rising after 7 Ma and having clear peaks at 2–3 Ma and after 1 Ma.

Temporal evolution in the first derivative of 565 nm shows some similar trends as 565/435 (Fig. 6). Both Bengal Fan sites (718 and U1451) show little temporal evolution, although 565 values at Site 718 are higher than seen at Site U1451. There is a period with variable and high values at 13–14.5 Ma. 565 values at Site U1456 (Indus) are similar to those at Site 718 but show a trend to higher values since 1.5 Ma. Sites 1146 and 1148 (Pearl River) show high values at 10–15 Ma and then decreased after 5 Ma. Values are higher at Site 1148 compared to Site 1146 because of the greater carbonate dilution at the latter site. Again, the long-term trend at Site U1433 (Mekong) is in the opposite direction since 8.5 Ma. With higher values after 5 Ma, more similar to the trend to higher values found at Site 1195 (East Australia), which is especially well defined after 6 Ma and reached maxima at 2–3 Ma and after 1 Ma.

Although redness (a*) is a less well reliable aridity proxy than 565/435 or 565 there is a close link to hematite content in those areas where both data sets exist (Fig. 3). The trend in a* at Site U1456 (Indus) is similar to the 565/435 record, showing an increase after 8 Ma, and high, variable values since ~3.5 Ma (Fig. 7). The Bengal Fan at Site 718 has lower a* values than measured at Site U1451, but both sites show no long-term trends, except for the variable and high values seen at 13–14.5 Ma at Site U1451. The a* record for the 90 East Ridge at Site U1443, also in the Bay of Bengal, is more coherent and shows high a* values through much of the Early and Middle Miocene, peaking at 17 Ma, then falling sharply from 13 to 8 Ma. After this there was a gentle rise to a modest peak at 5 Ma, and then another decrease until the recent. The reddening trend since 8 Ma mirrors that seen at Site U1456 (Indus). Likewise, the a* record for the Nicobar Fan (Site U1480) shows higher values after the start of fan sedimentation at ~9.5 Ma (McNeill et al. 2017a) and like its Bengal Fan neighbours has little long-term trend, beyond gently rising values since ~3 Ma.

The opposite trends seen at the Pearl and Mekong River sites are again apparent in the a* values, although the trend to higher a* values at Site U1433 (Mekong) after 5 Ma is less pronounced. Site U1430 (Sea of Japan) shows a long-term decline in a* values after a peak at 11–12 Ma. There is also a peak at 2–3 Ma before a fall and increasing variability since 2 Ma. At Site U1464 (NW Australia) there is also a long-term decline in values, reaching a minimum around 4 Ma, then rising

gradually to the present day. Site 1195 (Eastern Australia) shows the opposite trend, with a long-term rise, sharply at 6–7 Ma and especially at 2–3 Ma.

Evolution since 5 Ma

The last 5 m.y. were examined in detail in order to be better gauge the response of the Asia-Australian region to the onset of the Northern Hemisphere Glaciation (NHG) and the Mid Pleistocene Transition (MPT) (Berends et al. 2021). Figure 8 shows the last five million years of 565/435 records. It is apparent that Site U1456 (Indus Fan) has the highest 565/435 values of any of the records available. There was a period of a very high values between 1.6 and 1.0 Ma, with values falling after that time, approximately starting at the MPT. Many of the other records, particularly in the Pearl River (Sites 1146 and 1148) and Eastern Australia (Site 1195) show increasing variability and higher values, especially after ~1 Ma. Site U1433 (Mekong) also shows increasing values and greater variability after that time. The record at Site 718 (Bengal Fan) is rather discontinuous and shows no long-term change.

Considering only the 565 record (Fig. 9) the evolution in aridity appears a little different. In this case, the Indus Fan (Site U1456) shows higher hematite contents starting around 1.5 Ma. Eastern Australia (Site 1195) clearly has the highest 565 values overall and shows a very prominent peak between 3.2 and 2.2 Ma, essentially at the start of the NHG. This follows a low episode prior to 3.5 Ma. Another major rise to high values started around 0.7 Ma. Records from the Bengal Fan do not show any coherent variability, but generally have lower values than those seen in the Indus or in Eastern Australia. Site U1433 (Mekong) has higher 565 values than found in the Bengal or Pearl River catchments. As at Site 1195 (E Australia) there are lower values before ~2.5 Ma at Site U1433, followed by higher and more variable values since that time. The highest values are reached at the present day. The Pearl River sites (1146 and 1148) are both quite low in 565 values and show a decrease since 5 Ma, with slightly more variability seen since ~2 Ma.

Focusing on the a* records there is a general fall in values starting ~2 Ma at Site U1456 (Indus Fan), accompanied by more variability (Fig. 10). Site 718 (Bengal Fan) is too discontinuous to be useful, but Site U1451 shows a trend of modest decrease in a* from 5 Ma to ~3 Ma followed by an increase to higher and more variable values especially after 1.3 Ma. The same general pattern is also seen at Site U1443 (90 East Ridge), although with a particularly dramatic increase since 0.5 Ma. Site U1480 (Nicobar Fan) similarly has a sharp rise after 1.3 Ma, lower values from 0.9 to 0.5 Ma and then a rise to high values since 0.5 Ma, although this postdates the end of fan sedimentation, estimated at ~2 Ma (McNeill et al. 2017a). a* values are lower in South China Sea cores than seen

further west. Site U1433 (Mekong) shows a rise to higher and more variable values after 1.8 Ma. The two Pearl River sites (1146 and 1148) have similar long-term trends but differ from one another in detail. a* values are higher at Site 1148 and more variable after 2.3 Ma. The lower a* values at Site 1146 reflects the higher biogenic carbonate contents in those sediments, diluting the reddening effect of hematite (Wang et al. 2000a). The noisy record at the top of the Site 1148 section likely reflects the slumping noted in the seismic (Shipboard Scientific Party 2000). Site 1146 is much less variable and show very low values at 4.3–3.0 Ma and after 0.8 Ma. Modest differences in when the trends at Sites 1146 and 1148 change are likely caused by inconsistencies in the two age models, most notably in the low a* values at Site 1148 from 17 to 15 Ma but which are low at Site 1146 before 17 Ma, when those at Site 1148 were high. Site U1430 (Sea of Japan) shows rising values from 4.0 Ma to a peak at 2.8 Ma, a decrease to 1.7 Ma and then a steady increase and greater variability since that time. The Site U1464 record (NW Australia) is quite similar to that from the Sea of Japan and shows a well-defined trend to higher a* values. Eastern Australia (Site 1195) also increased from 4.5 Ma to the present day, but the rise is quite different in form, with a sharp increase between 3.3 and 2.0 Ma, followed by a low and another rise after 0.7 Ma.

Discussion

Interpretation of the 565/435 data is complicated because of what is implied by relative increases in hematite versus goethite. It might be supposed that higher concentrations of hematite would reflect drier or hotter conditions (Schwertmann & Taylor 1989). However, it is possible that greater hematite production could occur with increasing seasonality, when there was a well-defined dry season, rather than the climate being dry year-round. Supporting this view, some of the predicted high hematite values are known to be associated with wet conditions based on other proxies, at least in some regions, e.g., South China Sea (Fig. 2). This is consistent with the concept that high values of 565/435, really represent times of increased seasonality, a hallmark of the monsoon. For example, decreasing 565/435 values during the Late Miocene were seen offshore the Pearl River (Fig. 5), but at a time when salinity increased, implying less fluvial discharge and therefore weaker summer rains (Steinke et al. 2010). At the same time, the high 565/435 values at Site 1148 found during the Middle Miocene correlate with times of rapid erosion and fast sedimentation in the South China Sea (Clift 2006), generally interpreted to indicate the impact of strong monsoon.

Monsoon since 25 Ma

If the 565/435 proxy is interpreted in this way, the Indus basin had stronger seasonality than the drainage of the Bengal Fan, and reached maximum seasonality during the late Pliocene and Pleistocene (Fig. 5), albeit with an earlier Mid Miocene peak observed in southern China, following a gradual increase that started after 23 Ma. The Mid Miocene maximum lasted until ~11 Ma in southern China, followed by a steady decrease. It is noteworthy that the 565/435 proxy shows the opposite trend in the Mekong compared to the Pearl River since 10 Ma. Increasing seasonality in Indochina mirrors decreasing seasonality in the Pearl River basin. Liu *et al.* (2019) suggested that this may reflect a northwards migration of the ITCZ after 7 Ma. Isotope studies show higher salinity, less run-off and weaker rains at the same time during the Miocene in southern China (Steinke et al. 2010), along with less chemical weathering and erosion (Clift et al. 2014). Increased 565/435 values and thus seasonality in Eastern Australia, starting around 7 Ma and intensifying after 3 Ma is consistent with the general understanding of Australia becoming drier as it moved north and constricted the Indonesian Throughflow (Christensen et al. 2017). The higher seasonality also reflects drying of the Australian continent linked to long-term global cooling (Mao & Retallack 2019).

The 565 nm record has similar Implications for long-term climatic evolution as the 565/435 data but should be more reliable in those areas where the 435 nm data are unusable. The 565 nm record is helpful for understanding conditions in the Bengal Fan catchment in showing no major trend to drying or wettening beyond the variable and high 565 values (more seasonal) at 13–14.5 Ma and at 3–5 Ma at Site U1451. The reason for the differences between Sites 718 and U1451 is not clear but could reflect preferential transport of hematite further offshore, because the source of the sediment at the two sites is the same and does not change through the record, i.e., the Himalaya and foreland basin (Blum et al. 2018; Lenard et al. 2020). Indus Fan sediment generally has higher hematite contents than the Bengal Fan at Site U1451, but not more than at Site 718 (Fig. 6). The Indus Fan shows a trend to drying/more seasonal conditions from 10 to ~4.5 Ma, as well as after 1.5 Ma, some of which may reflect greater sediment supply from peninsular India after 1.5 Ma (Cai et al. 2020), and/or drier conditions associated with Northern Hemispheric Glaciation. The drying does not correlate with the provenance change towards more Himalayan erosion after ~6 Ma (Clift et al. 2019). However, the drying from 10 to 4.5 Ma is consistent with leaf wax δD isotopic values showing reduced precipitation along the Oman margin at that time (Huang et al. 2007), as well as interpretation of vegetation changes in the Siwalik Group foreland sedimentary rocks (Cerling et al. 1989). A parallel drying trend seen at Sites 1195 (East Australia) and U1433 (Mekong) since 8 Ma is apparent, especially at Site 1195 where a spectacular 565 peak is seen at 2–3 Ma, a feature not observed in any other area, but potentially linked to the migration of the Westerly Jet, as proposed during the Late Miocene in NW Australia (Groeneveld et al. 2017).

The a* records provide the best chance to compare records from all sites (Fig. 7). It is apparent that there is no simple pan-Asian trend to drying or wettening through the Neogene. The submarine fan deposits show some of the lowest degrees of coherent variability, especially the Bengal Fan. This may reflect the generally wetter conditions in the central and eastern Himalayan foreland through the Neogene compared to the west. Indeed, while a clear transition from C3 wood and shrub land to C4 grassland is seen in the Indus foreland during the Late Miocene (Feakins et al. 2020; Quade et al. 1989), there is no corresponding shift in the easternmost foreland basin (Vögeli et al. 2017), suggesting less drying in the Bengal catchment overall. The noisy character of the fan records is probably a function of their more variable lithologies, compared to muddy, distal locations. In contrast, Sites U1443 (90 East Ridge) and 1148 (Pearl River) show the greatest variations and most coherent histories. Both sites are dominated by hemipelagic sedimentation. Both show peak a* in the Early-Mid Miocene and then a decrease. The increase in a* values from ~25 Ma to 15 Ma is consistent with the rainfall modelling predictions of Thomson *et al.* (2021) that are largely driven by topographic uplift. The slow character of the change is suggestive of a tectonic trigger, because this mechanism is less likely to cause rapid change. The time of strongest monsoon seen at Sites U1443 (90 East Ridge) and 1148 (Pearl River) correlates with the time of Himalayan uplift brought on by Indian lithospheric tearing and slab break-off (Fig. 11)(Webb et al. 2017), closure of the Tethyan gateway between the Indian Ocean and Mediterranean Sea (Hamon et al. 2013), and the exposure of Arabia after early marine inundation (Sarr et al. 2022).

A subsequent decrease in a* values started earlier, after 12 Ma, on the 90 East Ridge but after 10 Ma in the Pearl River basin (Fig. 11). The decrease is however not predicted by the integrated modelling drawing on all possible forcing processes, although it would suggest that the influence of lower CO_2 levels is more important in South Asia that predicted. The decrease in monsoon rains after 15 Ma in eastern Asia may be linked to closure of the Tethyan gateway (Hamon et al. 2013) as well as the lower CO_2 concentrations, but also correlates with renewed surface uplift in the northern and SE Tibetan Plateau (Clark et al. 2005; Miao et al. 2022a). Closure of the Panama Gateway and strengthening of the Atlantic conveyer is predicted to have strengthening the South Asian Monsoon at ~5 Ma, although this is not observed on most of the Indian Ocean record, except with the increase in seasonality seen at Site U1143 (90 East Ridge).

Australian records show some contrasts with Asian records. Both NW and Eastern Australia exhibit long-term drying after 7 Ma, like the Indus, 90 East Ridge and Mekong, but different from the Pearl River. Australia itself is drier and more seasonal in the NW compared to the East prior to 7 Ma. The Site U1464 a* record does a good job of picking out the humid interval from 6.0 to 4.0 Ma

(Karatsolis et al. 2020), with the opposite seen in the Eastern Site 1195. Geochemical downhole logging data from Site U1464 showed year-round humidity at 4–6 Ma following by establishment of a more seasonal, monsoonal climate after 4 Ma (Christensen et al. 2017). Eastern Australia shows the closest similarity with the Mekong River. It is noteworthy that the humid interval at Site U1464 corresponds with a time of low a* values at Site U1433 (also at Site 1195). This contrasts with 90 East Ridge and South China Sea where low values are associated with strong summer monsoon rains. The different response of Australia compared to Asia likely reflects its low topography and lack of tectonic activity. Greater discharge resulted in faster transport and less chemical weathering in this case.

Monsoon Since 5 Ma

Focusing on the past 5 Ma the impact of onset of NHG and the MPT on continental environments can be assessed. 565/435 values increased at the onset of the NHG in the Mekong and in Eastern Australia and shortly after that time in southern China (Fig. 8). Increased seasonality is inferred to be linked to the establishment of the permanent northern hemispheric ice sheets. The MPT is also marked by drying in Eastern Australia and the Mekong but wettening in the Pearl River basin, consistent with ITCZ northward migration (Liu et al. 2019). There is a change to less seasonality in the Indus, but this may reflect a change in provenance at Site U1456 rather than true environmental change (Cai et al. 2020). The 565 nm proxy by itself shows little correlation with the global climate, except for there being more hematite in the Indus Fan after the MPT (Fig. 9). However, like 565/435, the a* proxy shows clearer environmental responses at the hemipelagic sites, if not from the Indus or Bengal fans. The 90 East Ridge shows increasing redness, linked to heightened seasonality after the onset of NHG, while at Site U1480 a* values were more variable after the NHG and a major peak at the MPT. It should be remembered that this was after the end of Nicobar Fan sedimentation, although sediment was still largely from the Bengal delta in hemipelagic form. Sites 1148 (Pearl River) and U1430 (Sea of Japan) show much greater variability and reduced redness after the MPT, suggestive of a weaker monsoon. In contrast, drying is inferred for NW Australia after the start of NHG and this becomes stronger again after the MPT. Deposition of very red sediment around the onset of NHG in Eastern Australia is indicative of drying and greater seasonality in that area starting at the MPT.

Synthesis

Figure 12 shows a simplified synthesis of the results discussed above using palaeogeographic reconstructions based on the plate tectonic model of Hall (2002). The Middle Miocene exhibited wet

monsoon conditions across south Asia and southern China, with moderately less humidity in SE Asia (Fig. 12D). At this time NW Australia was more seasonal and wetter than the east (Christensen et al. 2017). By 10 Ma (early Late Miocene) the monsoon rains were still strong in southern China but had started to weaken in the Bengal/Irrawaddy systems. Seasonal rainfall remained strong in Indochina. In Australia there was little change in the environment since 15 Ma, being drier in the west and wetter in the East (Fig. 12C). By 5 Ma in the Early Pliocene the "Humid Phase" had started in NW Australia (Karatsolis et al. 2020), and even Eastern Australia was still wet. In mainland Asia the Mekong was also humid, while southern China had started to experience weaker monsoon rains. The Sea of Japan seems to have been more monsoonal than it had been at 10 Ma. Likewise, the Indus Basin had started to dry, despite the lack of change in the Bengal Basin/Irrawaddy (Fig. 12B). Finally, looking at the Late Pleistocene (1 Ma), more short-term climatic variability is observed than before. The Indus and southern China were drier than before. The Bengal Fan shows little change, but the 90 East Ridge suggests moderate wettening in that region since the Pliocene. The Sea of Japan also displays modest change compared to the Pliocene, although with markedly greater variability. Both sides of Australia continued their trend to drier conditions (Fig. 12A).

Impacts on Vegetation

It might be expected that changing rainfall and seasonality would have an impact on the biosphere. The most reliable four environmental records of 565/435 can be used to see how changing seasonality and rainfall relate to changes in the vegetation, constrained by pollen data or by stable isotopes and in turn to photosynthetic pathways. Figure 13A shows that a gradual trend to higher hematite/goethite values in the Mekong basin since ~5.5 Ma, and especially after ~2.3 Ma, correlated with reduced proportions of ferns in the spore assemblage, as well as greater proportion of herb and conifer pollen (Miao et al. 2017). The latter in particular increased sharply after the start of the NHG and a spike in 565/435 values. In contrast, in the Arabian Sea the transition from tree and shrub-dominated (C3) to grass-dominated (C4) vegetation, as tracked by leaf wax carbon isotope and is known to occur after 7.2 Ma (Fig. 13B), which is a time of increasing 565/435, although not notably quickly at that time. Feakins *et al*. (2020) note that this transition did not correlate with significant change in δD values, which is a rainfall intensity proxy. This implies that the monsoon may not be the governing factor in driving this environmental change. Comparison of the 565/435 record in the Pearl River with new pollen data from a nearby drill site (Miao et al. 2022b) shows a good first order correlation between humidity and vegetation. Ferns, conifers and broadleaved trees are generally more abundant when the monsoon was strong in the Early and Middle Miocene (Fig. 12C). There is a modest increase in all three groups during the Pleistocene

when climatic variability increased during glacial cycles. Finally, in Eastern Australia increased seasonality started after 6 Ma and broadly correlates with higher proportions of Myrtaceae and conifer pollen in Queensland (Kershaw et al. 1994). Offshore stable isotope records from western Australia show a C3 to C4 transition starting ~3.5 Ma (Andrae et al. 2018) at a time of increased seasonality, as tracked by 565/435 (Fig. 13D). Monsoon intensity is often an important control on vegetation but does not always dominate. Like the monsoon itself the timing of vegetation change varies across the Indo-Pacific region and is not tied only to rainfall or to CO_2 concentrations (Tauxe & Feakins 2020).

Conclusions

DRS data from scientific drilling cores collected across the Asian marginal seas and the continental shelves of Australia provide a good opportunity to examine long-term trends in continental environments, particularly aridity and seasonality. Although some of the data from IODP is corrupted by poor quality low frequency intensities these records can be still used to look at abundances of hematite through the 565 nm proxy, as well as a* (redness) values. There is a strong correlation between redness and 565 nm intensity, suggesting that most redness in the sediment is caused by the presence of hematite, favoured by dryer or more seasonal conditions. There is a less well-defined connection between goethite and b* (blueness). It is apparent that hematite concentrations do not correlate to aridity or seasonality in a linear fashion but vary across the area depending on the landscape and tectonic setting. Other proxies are needed to assess whether the trends are linked to simple drying or more seasonality, which is a hallmark of the monsoon. The clearest, most coherent, sedimentary records are found at sites where the sedimentation is hemiplegic, on the 90 East Ridge (Site U1443), and in the northern South China Sea (Sites 1146 and 1148). Both these areas imply long-term drying of the climate in their source regions starting in the Late Miocene, with peak monsoon during the Early Miocene on the 90 East Ridge, and later during the Middle Miocene in the South China Sea. The gradual strengthening before that time likely reflected topographic growth of the Himalaya and Tibetan Plateau, as well as closure of the Tethyan Gateway. Weakening monsoon rainfall is controlled by global cooling since the Mid Miocene.

Records from the Indian Ocean submarine fans show little long-term trend, although there is a suggestion that the monsoon may have reached its peak in the sources of the Bengal Fan around 13–15 Ma. Records from the Indus Fan are consistent with that catchment drying after ~8 Ma, similar to source regions to the Sea of Japan, i.e., Central Asia. Site U1433 which is supplied by sediment from the Mekong River shows drying after ~5 Ma, the opposite trend displayed by the

Pearl River and indicative of a migration of the ITCZ across Southeast Asia to account for these opposing trends.

Climatic trends in Australia are largely independent of those seen in Asia, although in eastern Australia, there is evidence for a significant drying starting after ~3 Ma (Christensen et al. 2017; Karatsolis et al. 2020), following a wet phase at 3–5 Ma seen in NW and eastern Australia. Many sites show variable and drier conditions after ~1 Ma linked to the MPT. The climatic trends in Australia seems largely controlled by the northward drift of the continent through dryer mid latitudes and into wetter, more tropical conditions especially in the northwest. More recent drying of the Australian climate has been linked to the relatively recent reduction of the Indonesian Through-Flow (De Vleeschouwer et al. 2018). More generally drier conditions in the Pleistocene are likely related to the onset of NHG and a weakening of Earth's hydrologic cycle.

Comparison of the environmental records with pollen data constraining the nature of vegetation across the area imply significant control by the climate over the biosphere. Long-term drying in the Mekong basin resulted in increases in herbs and conifers at the expense of ferns (Miao et al. 2017). In the Pearl River basin wet conditions in the Middle Miocene correlate with peak concentrations of ferns and broadleaf vegetation, followed by drying in the Late Miocene. In eastern Australia, drying of the climate, since ~6 Ma correlated with increases in Myrtaceae and in conifers. However, the drying trend seen in the NW Himalayan foreland, and preserved in the Indus Fan does not correlate well with the transition from C3-dominated to C4-dominated conditions in that area, consistent with the idea that this transition is not only linked to the intensity of seasonality of rainfall (Tauxe & Feakins 2020).

Acknowledgements

PC thanks the Charles T. McCord Jr Chair in Petroleum Geology at LSU for support during this study. The Hanse Wissenschaftskolleg (Germany) and the University of Hong Kong are thanked for providing time and opportunity to think about these problems. The manuscript benefited from comments by Ziye Li, as well as from Guillaume Dupont-Nivet, Chris Morley and an anonymous reviewer.

Data availability

All data presented here are available from the IODP databank (https://web.iodp.tamu.edu/LORE/) for IODP wells or Janus (http://www-odp.tamu.edu/database/janusmodel.htm) for ODP wells.

References

Acosta, R.P. & Huber, M. 2017. The neglected Indo-Gangetic Plains low-level jet and its importance for moisture transport and precipitation during the peak summer monsoon. *Geophysical Research Letters*, **44**, 8601-8610, doi:10.1002/2017GL074440.

Acosta, R.P. & Huber, M. 2020. Competing Topographic Mechanisms for the Summer Indo-Asian Monsoon. *Geophysical Research Letters*, **47**, e2019GL085112, doi:10.1029/2019GL085112.

Ali, S., Hathorne, E.C. & Frank, M. 2021. Persistent Provenance of South Asian Monsoon-Induced Silicate Weathering Over the Past 27 Million Years. *Paleoceanography and Paleoclimatology*, **36**, e2020PA003909, doi:10.1029/2020PA003909.

An, Z., Kukla, G.J., Porter, S.C., Xiao, J. & Anonymous. 1991. Magnetic susceptibility evidence of monsoon variation on the Loess Plateau of central China during the last 130,000 years. *Quaternary Research (New York)*, **36**, 29-36.

Andrae, J.W., McInerney, F.A., Polissar, P.J., Sniderman, J.M.K., Howard, S., Hall, P.A. & Phelps, S.R. 2018. Initial Expansion of C4 Vegetation in Australia During the Late Pliocene. *Geophysical Research Letters*, **45**, 4831-4840, doi:10.1029/2018GL077833.

Balsam, W.L. & Damuth, J.E. 2000. Further investigations of shipboard vs. shore-based spectral data: implications for interpreting Leg 164 sediment composition. *In*: Paull, C.K., Matsumoto, R., Wallace, P.J. & Dillon, W.P. (eds.) *Proceedings of the Ocean Drilling Program, Scientific Results*. Ocean Drilling Program, College Station, TX, 313-324.

Balsam, W.L., Damuth, J.E., Schneider, R.R. & Fox, G.L. 1997. Comparison of shipboard vs. shore-based spectral data from Amazon fan cores : Implications for interpreting sediment composition. *Proceedings of the Ocean Drilling Program, Scientific Results* Ocean Drilling Program, College Station, TX, 193-215.

Bartoli, G., Sarnthein, M., Weinelt, M., Erlenkauser, H., Garbe-Schoenberg, D. & Lea, D.W. 2005. Final closure of Panama and the onset of Nothern Hemisphere glaciation. *Earth and Planetary Science Letters*, **237**, 33-44.

Berends, C.J., Köhler, P., Lourens, L.J. & van de Wal, R.S.W. 2021. On the Cause of the Mid-Pleistocene Transition. *Reviews of Geophysics*, **59**, e2020RG000727, doi:10.1029/2020RG000727.

Berry, G. & Reeder, M.J. 2014. Objective Identification of the Intertropical Convergence Zone: Climatology and Trends from the ERA-Interim. *Journal of Climate*, **27**, 1894-1909, doi:10.1175/jcli-d-13-00339.1.

Betzler, C., Eberli, G.P., Alvarez Zarikian, C.A. & Expedition 359 Scientists. 2017. *Maldives Monsoon and Sea Level.* International Ocean Discovery Program.

Betzler, C., Eberli, G.P., Kroon, D., Wright, J.D., Swart, P.K., Nath, B.N., Alvarez-Zarikian, C.A., Alonso-García, M., Bialik, O.M., Blättler, C.L., Guo, J.A., Haffen, S., Horozai, S., Inoue, M., Jovane, L., Lanci, L., Laya, J.C., Mee, A.L.H., Lüdmann, T., Nakakuni, M., Niino, K., Petruny, L.M., Pratiwi, S.D., Reijmer, J.J.G., Reolid, J., Slagle, A.L., Sloss, C.R., Su, X., Yao, Z. & Young, J.R. 2016. The abrupt onset of the modern South Asian Monsoon winds. *Scientific Reports*, **6**, doi:10.1038/srep29838.

Blum, M., Rogers, K., Gleason, J., Najman, Y., Cruz, J. & Fox, L. 2018. Allogenic and Autogenic Signals in the Stratigraphic Record of the Deep-Sea Bengal Fan. *Scientific Reports*, **8**, 7973, 10.1038/s41598-018-25819-5.

Boos, W.R. & Kuang, Z. 2010. Dominant control of the South Asian monsoon by orographic insulation versus plateau heating. *Nature*, **463**, 218-222, doi:10.1038/nature08707.

Bouquillon, A., France-Lanord, C., Michard, A. & Tiercelin, J. 1990. Sedimentology and isotopic chemistry of the Bengal Fan sediments: the denudation of the Himalaya. *In*:

Cochran, J.R., Stow, D.A.V. & Auroux, C. (eds.) *Proceedings of the Ocean Drilling Program, Scientific Results*. Ocean Drilling Program, College Station, TX, 43-58.

Bretschneider, L., Hathorne, E.C., Huang, H., Lübbers, J., Kochhann, K.G.D., Holbourn, A., Kuhnt, W., Thiede, R., Gebregiorgis, D., Giosan, L. & Frank, M. 2021. Provenance and Weathering of Clays Delivered to the Bay of Bengal During the Middle Miocene: Linkages to Tectonics and Monsoonal Climate. *Paleoceanography and Paleoclimatology*, **36**, e2020PA003917, doi:10.1029/2020PA003917.

Cai, M., Xu, Z., Clift, P.D., Khim, B.-K., Lim, D., Yu, Z., Kulhanek, D.K. & Li, T. 2020. Long-term history of sediment inputs to the eastern Arabian Sea and its implications for the evolution of the Indian summer monsoon since 3.7 Ma. *Geological Magazine*, **157**, 908-919, doi:10.1017/S0016756818000857.

Cai, M., Xu, Z., Clift, P.D., Lim, D., Khim, B.-K., Yu, Z., Kulhanek, D.K., Li, T., Chen, H. & Sun, R. 2019. Depositional History and Indian Summer Monsoon Controls on the Silicate Weathering of Sediment Transported to the Eastern Arabian Sea: Geochemical Records From IODP Site U1456 Since 3.8 Ma. *Geochemistry, Geophysics, Geosystems*, **20**, 4336-4353, doi:10.1029/2018GC008157.

Calvès, G., Huuse, M., Clift, P.D. & Brusset, S. 2015. Giant fossil mass wasting off the coast of West India: The Nataraja submarine slide. *Earth and Planetary Science Letters*, **432**, 265–272, doi:10.1016/j.epsl.2015.10.022.

Canfield, D.E., Raiswell, R. & Bottrell, S.H. 1992. The reactivity of sedimentary iron minerals toward sulfide. *American Journal of Science*, **292**, 659-683, doi:10.2475/ajs.292.9.659.

Caves Rugenstein, J.K. & Chamberlain, C.P. 2018. The evolution of hydroclimate in Asia over the Cenozoic: A stable-isotope perspective. *Earth-Science Reviews*, **185**, 1129-1156, doi:10.1016/j.earscirev.2018.09.003.

Cerling, T.E., Quade, J., Wang, Y. & Bowman, J.R. 1989. Carbon isotopes in soils and Palaeosols as ecology and palaeoecology indicators. *Nature (London)*, **341**, 138-139.

Christensen, B.A., Renema, W., Henderiks, J., De Vleeschouwer, D., Groeneveld, J., Castañeda, I.S., Reuning, L., Bogus, K., Auer, G., Ishiwa, T., McHugh, C.M., Gallagher, S.J. & Fulthorpe, C.S. 2017. Indonesian Throughflow drove Australian climate from humid Pliocene to arid Pleistocene. *Geophysical Research Letters*, **44**, 6914-6925, doi:10.1002/2017GL072977.

Clark, M.K., House, M.A., Royden, L.H., Whipple, K.X., Burchfiel, B.C., Zhang, X. & Tang, W. 2005. Late Cenozoic uplift of southeastern Tibet. *Geology*, **33**, 525-528, doi: 10.1130/G21265.1.

Clemens, S.C., Kuhnt, W., LeVay, L.J. & Shipboard Scientific Party. 2016. Site U1443. *Proceedings of the International Ocean Discovery Program* **353**, doi:10.14379/iodp.proc.353.103.2016.

Clift, P., Lee, J.I., Clark, M.K. & Blusztajn, J. 2002. Erosional response of south China to arc rifting and monsoonal strengthening; a record from the South China Sea. *Marine Geology*, **184**, 207-226, doi:10.1016/S0025-3227(01)00301-2.

Clift, P.D. 2006. Controls on the erosion of Cenozoic Asia and the flux of clastic sediment to the ocean. *Earth and Planetary Science Letters*, **241**, 571-580, doi:10.1016/j.epsl.2005.11.028.

Clift, P.D., Betzler, C., Clemens, S.C., Christensen, B., Eberli, G.P., France-Lanord, C., Gallagher, S., Holbourn, A., Kuhnt, W., Murray, R.W., Rosenthal, Y., Tada, R. & Wan, S. 2022. A synthesis of monsoon exploration in the Asian marginal seas. *Scientific Drilling*, **10**, 1-29, doi:10.5194/sd-10-1-2022.

Clift, P.D., Wan, S. & Blusztajn, J. 2014. Reconstructing Chemical Weathering, Physical Erosion and Monsoon Intensity since 25 Ma in the northern South China Sea: A review

of competing proxies. *Earth-Science Reviews*, **130**, 86-102, doi:10.1016/j.earscirev.2014.01.002.

Clift, P.D., Zhou, P., Stockli, D.F. & Blusztajn, J. 2019. Regional Pliocene exhumation of the Lesser Himalaya in the Indus drainage. *Solid Earth*, **10**, 647-661, doi:10.5194/se-10-647-2019.

Curry, W.B., Ostermann, D.R., Guptha, M.V.S. & Itekkot, V. 1992. Foraminiferal production and monsoonal upwelling in the Arabian Sea; evidence from sediment traps. *In*: Summerhayes, C.P., Prell, W.L. & Emeis, K.C. (eds.) *Upwelling systems; evolution since the early Miocene*. Geological Society, London, Special Publication, 93–106.

De Vleeschouwer, D., Auer, G., Smith, R., Bogus, K., Christensen, B., Groeneveld, J., Petrick, B., Henderiks, J., Castañeda, I.S., O'Brien, E., Ellinghausen, M., Gallagher, S.J., Fulthorpe, C.S. & Pälike, H. 2018. The amplifying effect of Indonesian Throughflow heat transport on Late Pliocene Southern Hemisphere climate cooling. *Earth and Planetary Science Letters*, **500**, 15-27, doi:10.1016/j.epsl.2018.07.035.

Deaton, B.C. & Balsam, W.L. 1991. Visible Spectroscopy - a rapid method for determining hematite and goethite concentration in geological materials. *Journal of Sedimentary Petrology*, **61**, 628-632.

Ehlers, T.A., Chen, D., Appel, E., Bolch, T., Chen, F., Diekmann, B., Dippold, M.A., Giese, M., Guggenberger, G., Lai, H.-W., Li, X., Liu, J., Liu, Y., Ma, Y., Miehe, G., Mosbrugger, V., Mulch, A., Piao, S., Schwalb, A., Thompson, L.G., Su, Z., Sun, H., Yao, T., Yang, X., Yang, K. & Zhu, L. 2022. Past, present, and future geo-biosphere interactions on the Tibetan Plateau and implications for permafrost. *Earth-Science Reviews*, **234**, 104197, doi:10.1016/j.earscirev.2022.104197.

Farnsworth, A., Lunt, D.J., Robinson, S.A., Valdes, P.J., Roberts, W.H.G., Clift, P.D., Markwick, P., Su, T., Wrobel, N., Bragg, F., Kelland, S.-J. & Pancost, R.D. 2019. Past East Asian monsoon evolution controlled by paleogeography, not CO2. *Science Advances*, **5**, eaax1697, doi:10.1126/sciadv.aax1697.

Feakins, S.J., Liddy, H.M., Tauxe, L., Galy, V., Feng, X., Tierney, J.E., Miao, Y. & Warny, S. 2020. Miocene C4 Grassland Expansion as Recorded by the Indus Fan. *Paleoceanography and Paleoclimatology*, **35**, e2020PA003856, doi:10.1029/2020PA003856.

France-Lanord, C., Derry, L. & Michard, A. 1993. Evolution of the Himalaya since Miocene time: Isotopic and sedimentologic evidence from the Bengal Fan *In*: Treloar, P.J. & Searle, M.P. (eds.) *Himalayan Tectonics*. Geological Society, London, Special Publications, 603–621.

France-Lanord, C., Spiess, V., Klaus, A. & Expedition 354 Scientists. 2015. Bengal Fan: Neogene and late Paleogene record of Himalayan orogeny and climate: a transect across the Middle Bengal Fan. *International Ocean Discovery Program Preliminary Report*, **354**, doi:10.14379/iodp.pr.354.2015.

Gallagher, S.J., Fulthorpe, C.S., Bogus, K. & Party, S.S. 2017. Site U1464. *Proceedings of the International Ocean Discovery Program*, doi:10.14379/iodp.proc.356.109.2017.

Giosan, L., Flood, R.D., Grutzner, J. & Mudie, P. 2002. Paleoceanographic significance of sediment color on western North Atlantic Drifts: II. Late Pliocene-Pleistocene sedimentation. *Marine Geology*, **189**, 43-61.

Godin, L., Grujic, D., Law, R.D. & Searle, M.P. 2006. Channel flow, ductile extrusion and exhumation in continental collision zones; an introduction. *In*: Law, R.D., Searle, M.P. & Godin, L. (eds.) *Channel Flow, Ductile Extrusion, and Exhumation of Lower-Middle Crust in Continental Collision Zones*. Geological Society, London, Special Publication, 1-23.

Gordon, A.L. 2005. Oceanography of the Indonesian seas and their throughflow. *Oceanography*, **18**, 14–27, doi:10.5670/oceanog.

Gradstein, F.M., Ogg, J.G., Schmitz, M.D. & Ogg, G.M. 2020. Geologic Time Scale 2020. Elsevier Science.

Groeneveld, J., Henderiks, J., Renema, W., McHugh, C.M., Vleeschouwer, D.D., Christensen, B.A., Fulthorpe, C.S., Reuning, L., Gallagher, S.J., Bogus, K., Auer, G. & Ishiwa, T. 2017. Australian shelf sediments reveal shifts in Miocene Southern Hemisphere westerlies. *Science Advances*, **3**, e1602567, doi:10.1126/sciadv.1602567.

Hall, R. 2002. Cenozoic geological and plate tectonic evolution of SE Asia and the SW Pacific: computer-based reconstructions and animations. *Journal of Asian Earth Sciences*, **20**, 353-434, doi:10.1016/S1367-9120(01)00069-4.

Hamon, N., Sepulchre, P., Lefebvre, V. & Ramstein, G. 2013. The role of eastern Tethys seaway closure in the Middle Miocene Climatic Transition (ca. 14 Ma). *Clim. Past*, **9**, 2687-2702, doi:10.5194/cp-9-2687-2013.

Hoang, L.V., Clift, P.D., Schwab, A.M., Huuse, M., Nguyen, D.A. & Zhen, S. 2010. Large-scale erosional response of SE Asia to monsoon evolution reconstructed from sedimentary records of the Song Hong-Yinggehai and Qiongdongnan Basins, South China Sea. *In*: Clift, P.D., Tada, R. & Zheng, H. (eds.) *Monsoon evolution and tectonic-climate linkage in Asia*. Geological Society, London, Special Publication, 219–244.

Hu, D., Böning, P., Köhler, C.M., Hillier, S., Pressling, N., Wan, S., Brumsack, H.-J. & Clift, P.D. 2012. Deep sea records of the continental weathering and erosion response to East Asian monsoon intensification since 14ka in the South China Sea. *Chemical Geology*, **326-327**, 1-18, doi:10.1016/j.chemgeo.2012.07.024.

Huang, Y., Clemens, S.C., Liu, W., Wang, Y. & Prell, W.L. 2007. Large-scale hydrological change drove the late Miocene C4 plant expansion in the Himalayan foreland and Arabian Peninsula. *Geology*, **35**, 531-534, doi:10.1130/G23666A.1.

Isern, A.R., Anselmetti, F.S., Blum, P. & Shipboard Scientific Party. 2002. Site 1195. *Proceedings of the Ocean Drilling Program, Part A: Initial Reports*, **194**, doi:10.2973/odp.proc.ir.194.106.2002.

Ji, J., Balsam, W., Chen, J. & Liu, L. 2002. Rapid and quantitative measurement of hematite and goethite in the Chinese Loess-Paleosol sequences by diffuse reflectance spectroscopy. *Clays and Clay Minerals*, **50**, 208-216.

Karatsolis, B.-T., De Vleeschouwer, D., Groeneveld, J., Christensen, B. & Henderiks, J. 2020. The Late Miocene to Early Pliocene "Humid Interval" on the NW Australian Shelf: Disentangling Climate Forcing From Regional Basin Evolution. *Paleoceanography and Paleoclimatology*, **35**, e2019PA003780, doi:10.1029/2019PA003780.

Kershaw, A.P., Martin, H.A. & Mason, J.R.C.M. 1994. The Neogene a period of transition. *In*: Hill, R.S. (ed.) *History of the Australian Vegetation*. University of Adelaide Press, Cretaceous to Recent, 299-327.

Kortüm, G., Braun, W. & Herzog, G. 1963. Principles and Techniques of Diffuse-Reflectance Spectroscopy. *Angewandte Chemie International Edition in English*, **2**, 333-341, doi:10.1002/anie.196303331.

Kosmas, C.S., Franzmeier, D.P. & Schulze, D.G. 1986. Relationship Among Derivative Spectroscopy, Color, Crystallite Dimensions, and Al Substitution of Synthetic Goethites and Hematites. *Clays and Clay Minerals*, **34**, 625-634, doi:10.1346/CCMN.1986.0340602.

Kroon, D., Steens, T. & Troelstra, S.R. 1991. Onset of Monsoonal related upwelling in the western Arabian Sea as revealed by planktonic foraminifers. *In*: Prell, W. & Niitsuma,

N. (eds.) *Proceedings of the Ocean Drilling Program, Scientific Results*. Ocean Drilling Program, College Station, TX, 257–263.
Kutzbach, J.E., Prell, W.L. & Ruddiman, W.F. 1993. Sensitivity of Eurasian climate to surface uplift of the Tibetan Plateau. *Journal of Geology*, **101**, 177–190.
Lenard, S.J.P., Lavé, J., France-Lanord, C., Aumaître, G., Bourlès, D.L. & Keddadouche, K. 2020. Steady erosion rates in the Himalayas through late Cenozoic climatic changes. *Nature Geoscience*, **13**, 448-452, doi:10.1038/s41561-020-0585-2.
Li, C.-F., Lin, J., Kulhanek, D.K. & Expedition 349 Scientists. 2015. *Proceedings of the International Ocean Discovery Program, 349: South China Sea Tectonics.* International Ocean Discovery Program.
Lisiecki, L.E. & Raymo, M.E. 2005. A Pliocene-Pleistocene stack of 57 globally distributed benthic d18O records. *Paleoceanography*, **20**, PA1003, doi:10.1029/2004PA001071.
Liu, C., Clift, P.D., Giosan, L., Miao, Y., Warny, S. & Wan, S. 2019. Paleoclimatic evolution of the SW and NE South China Sea and its relationship with spectral reflectance data over various age scales. *Palaeogeography, Palaeoclimatology, Palaeoecology*, **525**, 25-43, doi:10.1016/j.palaeo.2019.02.019.
Liu, C., Clift, P.D., Murray, R.W., Blusztajn, J., Ireland, T., Wan, S. & Ding, W. 2017. Geochemical Evidence for Initiation of the Modern Mekong Delta in the southwestern South China Sea after 8 Ma. *Chemical Geology*, **451**, 38–54, doi:10.1016/j.chemgeo.2017.01.008.
Liu, C., Stockli, D.F., Clift, P.D., Wan, S., Stockli, L.D., Höfig, T.W. & Schindlbeck-Belo, J.C. 2022. Geochronological and geochemical characterization of paleo-rivers deposits during rifting of the South China Sea. *Earth and Planetary Science Letters*, **584**, 117427, doi:10.1016/j.epsl.2022.117427.
Mao, X. & Retallack, G. 2019. Late Miocene drying of central Australia. *Palaeogeography, Palaeoclimatology, Palaeoecology*, **514**, 292-304, doi:10.1016/j.palaeo.2018.10.008.
McNeill, L.C., Dugan, B., Backman, J., Pickering, K.T., Pouderoux, H.F.A., Henstock, T.J., Petronotis, K.E., Carter, A., Chemale, F., Milliken, K.L., Kutterolf, S., Mukoyoshi, H., Chen, W., Kachovich, S., Mitchison, F.L., Bourlange, S., Colson, T.A., Frederik, M.C.G., Guèrin, G., Hamahashi, M., House, B.M., Hüpers, A., Jeppson, T.N., Kenigsberg, A.R., Kuranaga, M., Nair, N., Owari, S., Shan, Y., Song, I., Torres, M.E., Vannucchi, P., Vrolijk, P.J., Yang, T., Zhao, X. & Thomas, E. 2017a. Understanding Himalayan erosion and the significance of the Nicobar Fan. *Earth and Planetary Science Letters*, **475**, 134-142, doi:10.1016/j.epsl.2017.07.019.
McNeill, L.C., Dugan, B., Petronotis, K.E. & Expedition 362 Scientists. 2017b. Sumatra Subduction Zone. *Proceedings of the International Ocean Discovery Program*, **362**, doi:/10.14379/iodp.proc.362.2017.
Miao, Y., Fang, X., Sun, J., Xiao, W., Yang, Y., Wang, X., Farnsworth, A., Huang, K., Ren, Y., Wu, F., Qiao, Q., Zhang, W., Meng, Q., Yan, X., Zheng, Z., Song, C. & Utescher, T. 2022a. A new biologic paleoaltimetry indicating Late Miocene rapid uplift of northern Tibet Plateau. *Science*, **378**, 1074-1079, doi:10.1126/science.abo2475.
Miao, Y., Herrmann, M., Wu, F., Yan, X. & Yang, S. 2012. What controlled Mid–Late Miocene long-term aridification in Central Asia? — Global cooling or Tibetan Plateau uplift: A review. *Earth-Science Reviews*, **112**, 155-172, doi:10.1016/j.earscirev.2012.02.003.
Miao, Y., Warny, S., Liu, C., Yang, Y., Lei, Y., Xiang, M. & Wang, Z. 2022b. Palynomorph assemblages evidence for river reorganization 8.5 million years ago in Southeast Asia. *Global and Planetary Change*, **212**, 103808, doi:10.1016/j.gloplacha.2022.103808.
Miao, Y.F., Warny, S., Liu, C., Clift, P.D. & Gregory, M. 2017. Neogene fungal record from IODP Site U1433, South China Sea: Implications for paleoenvironmental change and

the onset of the Mekong River. *Marine Geology*, **394**, 69-81, doi:10.1016/j.margeo.2017.05.007.
Nesbitt, H.W., Markovics, G. & Price, R.C. 1980. Chemical processes affecting alkalis and alkaline earths during continental weathering. *Geochimica et Cosmochimica Acta*, **44**, 1659–1666.
Pandey, D.K., Clift, P.D., Kulhanek, D.K. & Expedition 355 Scientists. 2016. Arabian Sea Monsoon. *Proceedings of the International Ocean Discovery Program*, **355**, doi:10.14379/iodp.proc.355.2016.
Quade, J., Cerling, T.E. & Bowman, J.R. 1989. Development of Asian monsoon revealed by marked ecological shift during the latest Miocene in northern Pakistan. *Nature*, **342**, 163-166, doi:10.1038/342163a0.
Roberts, A.P. 2015. Magnetic mineral diagenesis. *Earth-Science Reviews*, **151**, 1-47, doi:10.1016/j.earscirev.2015.09.010.
Routledge, C.M., Kulhanek, D.K., Tauxe, L., Scardia, G., Singh, A.D., Steinke, S., Griffith, E.M. & Saraswat, R. 2020. Revised geological timescale for IODP Sites U1456 and U1457. *Geological Magazine*, **157**, 961-978, doi:10.1017/S0016756819000104.
Sangode, S.J. & Bloemendal, J. 2004. Pedogenic transformation of magnetic minerals in Pliocene–Pleistocene palaeosols of the Siwalik Group, NW Himalaya, India. *Palaeogeography, Palaeoclimatology, Palaeoecology*, **212**, 95–118.
Sarr, A.-C., Donnadieu, Y., Bolton, C.T., Ladant, J.-B., Licht, A., Fluteau, F., Laugié, M., Tardif, D. & Dupont-Nivet, G. 2022. Neogene South Asian monsoon rainfall and wind histories diverged due to topographic effects. *Nature Geoscience*, **15**, 314-319, doi:10.1038/s41561-022-00919-0.
Schwertmann, U. 1971. Transformation of hematite to goethite in soils. *Nature*, **232**, 624–625.
Schwertmann, U. & Taylor, R.M. 1989. Iron oxides. *In*: Dixon, J.B. & Weed, S.B. (eds.) *Minerals in Soil Environments*. Soil Society of America, Madison, WI, 379–438.
Shipboard Scientific Party. 1989. Site 718. *In*: Cochran, J.R. & Stow, D.A.V. (eds.) *Proceedings of the Ocean Drilling Program, Part A: Initial Reports*. Ocean Drilling Program, College Station, TX, 91-154.
Shipboard Scientific Party. 2000. Site 1148. *Proceedings of the Ocean Drilling Program, Part A: Initial Reports*.
Steinke, S., Groeneveld, J., Johnstone, H. & Rendle-Bühring, R. 2010. East Asian summer monsoon weakening after 7.5 Ma: Evidence from combined planktonic foraminifera Mg/Ca and δ18O (ODP Site 1146; northern South China Sea). *Palaeogeography, Palaeoclimatology, Palaeoecology*, **289**, 33-43, doi:10.1016/j.palaeo.2010.02.007.
Sun, X. & Wang, P. 2005. How old is the Asian monsoon system? Palaeobotanical records from China. *Palaeogeography, Palaeoclimatology, Palaeoecology*, **222**, 181-222, doi:10.1016/j.palaeo.2005.03.005.
Tada, R., Murray, R.W., Alvarez Zarikian, C.A. & Expedition 346 Scientists. 2015. *Asian Monsoon: onset and evolution of millennial-scale variability of Asian Monsoon and its possible relation with Himalaya and Tibetan plateau.* Integrated Ocean Drilling Program.
Tauxe, L. & Feakins, S.J. 2020. A Reassessment of the Chronostratigraphy of Late Miocene C3–C4 Transitions. *Paleoceanography and Paleoclimatology*, **35**, e2020PA003857, doi:10.1029/2020PA003857.
Thomson, J.R., Holden, P.B., Anand, P., Edwards, N.R., Porchier, C.A. & Harris, N.B.W. 2021. Tectonic and climatic drivers of Asian monsoon evolution. *Nature Communications*, **12**, 4022, doi:10.1038/s41467-021-24244-z.

Trenberth, K.E., Smith, L., Qian, T., Dai, A. & Fasullo, J. 2007. Estimates of the Global Water Budget and Its Annual Cycle Using Observational and Model Data. *Journal of Hydrometeorology*, **8**, 758-769, doi:10.1175/jhm600.1.

Vögeli, N., Najman, Y., van der Beek, P., Huyghe, P., Wynn, P.M., Govin, G., Veen, I.v.d. & Sachse, D. 2017. Lateral variations in vegetation in the Himalaya since the Miocene and implications for climate evolution. *Earth and Planetary Science Letters*, **471**, 1–9, doi:10.1016/j.epsl.2017.04.037.

Wan, S., Li, A., Clift, P.D. & Stuut, J.-B.W. 2007. Development of the East Asian monsoon: Mineralogical and sedimentologic records in the northern South China Sea since 20 Ma. *Palaeogeography, Palaeoclimatology, Palaeoecology*, **254**, 561–582, doi:10.1016/j.palaeo.2007.07.009.

Wang, B. 2006. The Asian Monsoon. Springer-Verlag, Berlin, 795.

Wang, P., Prell, W.L., Blum, P. & Shipboard Scientific Party. 2000a. Site 1146. *Proceedings of the Ocean Drilling Program, Part A: Initial Reports*, doi:10.2973/odp.proc.ir.184.107.2000.

Wang, P., Prell, W.L., Blum, P. & Shipboard Scientific Party. 2000b. Site 1148. *Proceedings of the Ocean Drilling Program, Part A: Initial Reports*, **184**, 121, doi:10.2973/odp.proc.ir.184.109.2000.

Webb, A.A.G., Guo, H., Clift, P.D., Husson, L., Müller, T., Costantino, D., Yin, A., Xu, Z., Cao, H. & Wang, Q. 2017. The Himalaya in 3D: Slab dynamics controlled mountain building and monsoon intensification. *Lithosphere*, doi:10.1130/L636.1.

Webster, P.J. 1987. The elementary monsoon. *In*: Fein, J.S. & Stephens, P.L. (eds.) *Monsoons*. John Wiley, New York, 3-32.

Wei, G., Li, X.-H., Liu, Y., Shao, L. & Liang, X. 2006. Geochemical record of chemical weathering and monsoon climate change since the early Miocene in the South China Sea. *Paleoceanography*, **21, PA4214**, doi:10.1029/2006PA001300.

Westerhold, T., Marwan, N., Drury, A.J., Liebrand, D., Agnini, C., Anagnostou, E., Barnet, J.S.K., Bohaty, S.M., De Vleeschouwer, D., Florindo, F., Frederichs, T., Hodell, D.A., Holbourn, A.E., Kroon, D., Lauretano, V., Littler, K., Lourens, L.J., Lyle, M., Pälike, H., Röhl, U., Tian, J., Wilkens, R.H., Wilson, P.A. & Zachos, J.C. 2020. An astronomically dated record of Earth's climate and its predictability over the last 66 million years. *Science*, **369**, 1383-1387, doi:10.1126/science.aba6853.

Zhang, Y.G., Jia, J., Balsam, W.L., Liu, L. & Chen, J. 2007. High resolution hematite and goethite records from ODP 1143, South China Sea: Co-evolution of monsoonal precipitation and El Niño over the past 600,000 years. *Earth and Planetary Science Letters*, **264**, 136-150, doi:10.1016/j.epsl.2007.09.022.

Zhou, P., Ireland, T., Murray, R.W. & Clift, P.D. 2021. Marine Sedimentary Records of Chemical Weathering Evolution in the Western Himalaya since 17 Ma. *Geosphere*, **17**, 824–853, doi:10.1130/GES02211.1.

Figure Captions

Figure 1. Shaded bathymetric map of the regions affected by the Asian and Australian monsoon systems showing the drill sites considered in this study, the location of the Intertropical convergence zone in each hemispheric summer, the location of the Westerly Jet in each hemisphere and the major oceanic currents affecting the Asian marginal seas. Route of Indonesian Throughflow after Gordon (2005).

Figure 2. Compilation of erosion and weathering proxies spanning 25 Ma at ODP Sites 1146 and 1148. (A) Smectite/kaolinite from Wan *et al*. (2007), (B) K/Al as a measure of chemical weathering intensity from the data of Wei *et al.* (2006), (C) Scanned Ti/Ca from ODP Site 1148 (Hoang et al. 2010), (D) $^{87}Sr/^{86}Sr$ values from ODP Site 1148, (E) the 565/435 proxy tracking the relative abundance of hematite vs goethite, (F) Magnetic susceptibility at Site 1148, and (G) Pollen proxies from central Asia (Sun & Wang 2005).

Figure 3. A) Cross plot of a* against the first derivative at 565 nm showing the close correlation between these proxies for all sediment spectral data in this study. B) Cross plot of a* against b* showing the separation seen between sediments in different areas. High a* values are especially common on the 90 East Ridge and Pearl River mouth, while high b* is limited to Eastern Australia and the Mekong basin.

Figure 4. A) Cross plot of a* against the first derivative at 435 nm (goethite proxy) showing the lack of any correlation between these proxies for all sediment spectral data in this study. B) Cross plot of b* against the first derivative at 435 nm showing a weak correlation between b* and goethite, best displayed in Eastern Australia.

Figure 5. Plots showing the temporal evolution in 565/435 values across Asia spanning from West (left) to East (right) since 25 Ma. Note the noisy record for the Bengal Fan Site U1451, demonstrating the poor quality of the data related to 435 nm wavelength at that site. All the data plotted represent 10 point running averages in order to eliminate extreme values and provide a smoother long-term record. The coloured bar to the left of the data provides a depiction of the average values for a given interval.

Figure 6. Plots showing the temporal evolution in 565 nm intensity, representing hematite abundance, across the Indo-Australian marginal seas since 25 Ma. With this proxy some Bengal Fan records gave coherent trends because this proxy was more stable than 435 nm. Many of the plots are similar to those shown in Figure 5. There is a common peak in 565 around 13–17 Ma in Asia, contrasting with the data from eastern Australia. Data are compared with the temperature of the

ocean, proxied by the benthic foraminifer oxygen isotope data from Westerhold *et al.* (2020). The coloured bar to the left of each plot provides a depiction of the average values for a given interval.

Figure 7. Plot of a* values for all the studied sections since 25 Ma. As a simple proxy this is available for all the drilled marginal basins. The 90 East Ridge has the reddest section but is also the most condensed. The Bengal Fan, Mekong and Pearl River sections show a tendency to maximum redness in the 13–17 Ma period. The Indus and Eastern Australian sections show increasing redness since 4 Ma. The coloured bar to the left of the data provides a depiction of the average values for a given interval.

Figure 8. Plots showing the temporal evolution in 565/435 data across Asia spanning since 5 Ma. Note that hematite/goethite values increased since 1.3 Ma in southern China and Australia, but is out of phase with other basins. The Indus is unusual in decreasing after a peak at 1.2–1.5 Ma. The benthic foraminifer stack of $\delta^{18}O$ values are from Lisiecki & Raymo (2005). The coloured bar to the left of the data provides a depiction of the average values for a given interval.

Figure 9. Plots showing the temporal evolution in 565 nm intensity across Asia since 5 Ma. Note how much more intense the record in Australia is compared to other regions, as well as the increased hematite response in the Indus Fan since ~1.2 Ma. The benthic foraminifer stack of $\delta^{18}O$ values is from Lisiecki & Raymo (2005). The coloured bar to the left of the data provides a depiction of the average values for a given interval.

Figure 10. Plot of a* for all the studied sections since 5 Ma. The 90 East Ridge, Nicobar Fan and Eastern Australia have the reddest sections. An intense red phase from 3.2 to 2.0 Ma is strikingly developed in Eastern Australia, is less well developed in NW Australia and is also recognized in the Sea of Japan. The benthic foraminifer stack of $\delta^{18}O$ values is from Lisiecki & Raymo (2005).

Figure 11. a* temporal records with the clearest patterns from South Asia (Site U1443), SE Asia (Site U1433) and East Asia (Site 1148) showing the timing of major vegetation changes, as well as significant climatic and tectonic events. Benthic foraminiferal oxygen isotopes are a proxy for seawater temperatures and are from Westerhold *et al*. (2020). Tethyan gateway closure age is from Hamon *et al.* (2013), Indian slab tearing is from Webb *et al.* (2017), motion on Main Central Thrust (MCT) is from Godin *et al.* (2006), Arabia exposure age is from Sarr *et al.* (2022), SE Tibet uplift is from Clark *et al.* (2005), Panama gateway closure is from Bartoli *et al.* (2005).

Figure 12. Simplified climatic evolution of the Asian-Australian monsoon region based on the 565 nm record and superimposed on the palaeogeography of Hall (2002). The coloured bar to the left of the

data provides a depiction of the average values for a given interval. This proxy is interpreted to reflect intensity of seasonal rainfall linked to a monsoon climate, rather than year-round humidity.

Figure 13. Comparison of the 565/435 records from four critical catchments compared to records of the evolving vegetation. A) Mekong with pollen data from IODP Site 1433 (Miao et al. 2017). B) Arabian Sea, Site U1456, with microfossil content and carbon isotope values from Feakins *et al.* (2020). C) Pearl River with pollen data from IODP Site U1499 (Miao et al. 2022b). D) Eastern Australia with pollen data from Kershaw *et al*. (1994).

Table Caption

Table 1. Summary of major climate events and states across Asia-Australia region deduced from the spectral records presented here.

Time	NW Himalaya	Central and Eastern Himalaya	Indochina	South China	NE Asia	Western Australia	Eastern Australia
Pleistocene	Modest wettening, variable monsoon	Variable monsoon	Variable monsoon	Modest wettening, variable monsoon	Variable and weak monsoon	Progressive drying	Variable weak monsoon
Pliocene	Peak aridity	Modest wettening	Progressive wettening after 5 Ma	Peak aridity at ~4 Ma	Progressive drying	Peak humidity 4-6 Ma	Variable weak monsoon
Late Miocene	Progressive drying	Peak aridity at 8-9 Ma	Progressive drying	Progressive drying after 10 Ma	Progressive drying	Progressive wettening	Strong drying after 6 Ma
Mid Miocene	Peak monsoon rain fall	Progressive drying after 12 Ma	Unknown	Peak monsoon rain fall ~15 Ma, tropical 15-17 Ma	Unknown	Dry climate	Peak monsoon rain fall, dry after 12 Ma
Early Miocene	Increasing rain fall	Peak rain fall ~18 Ma	Unknown	Increasing rain fall after 23 Ma	Unknown	Unknown	Humid climate
Oligocene	Unknown	Increasing rain fall	Unknown	Unknown	Unknown	Unknown	Unknown

Table 1

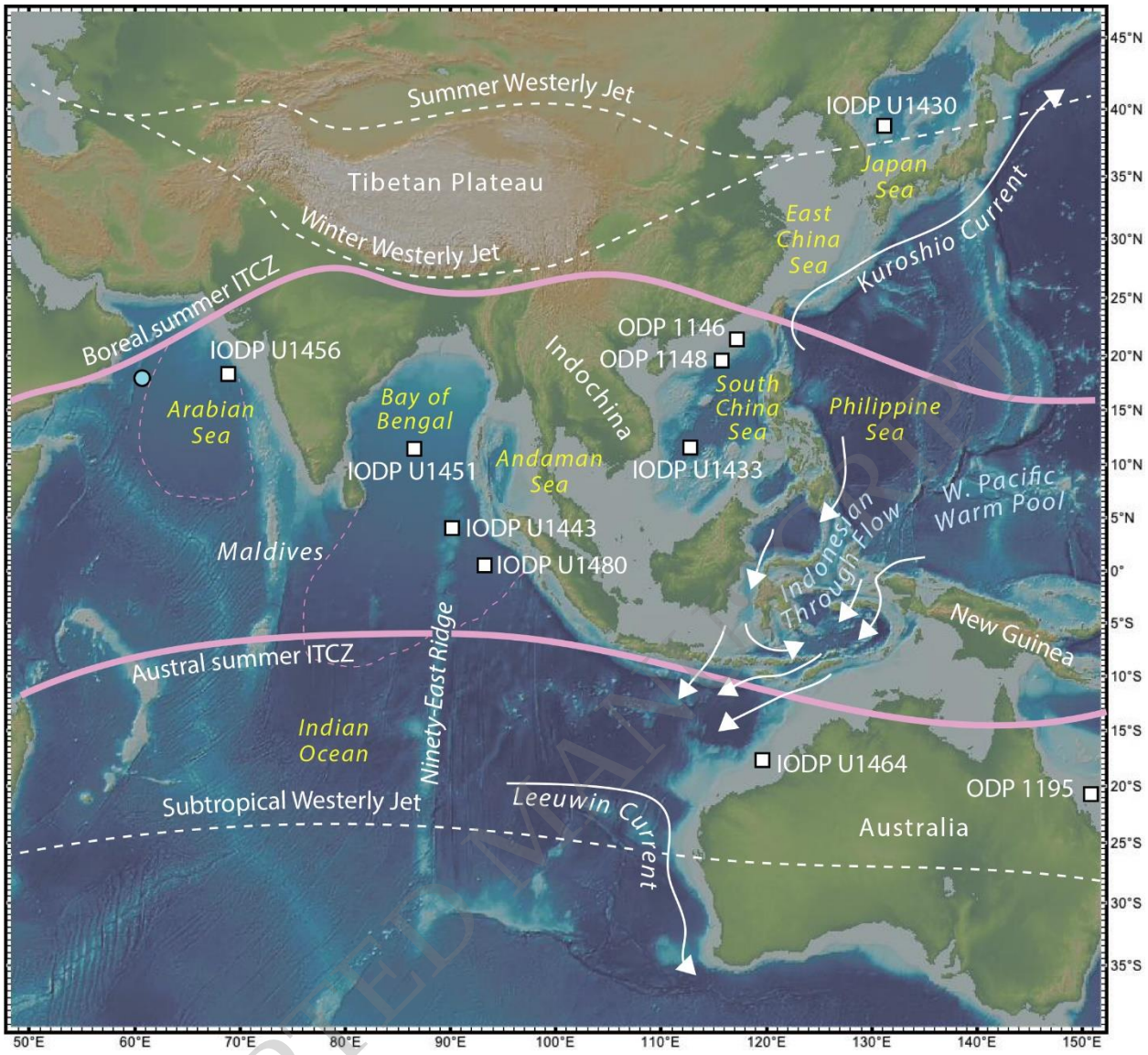

Figure 1

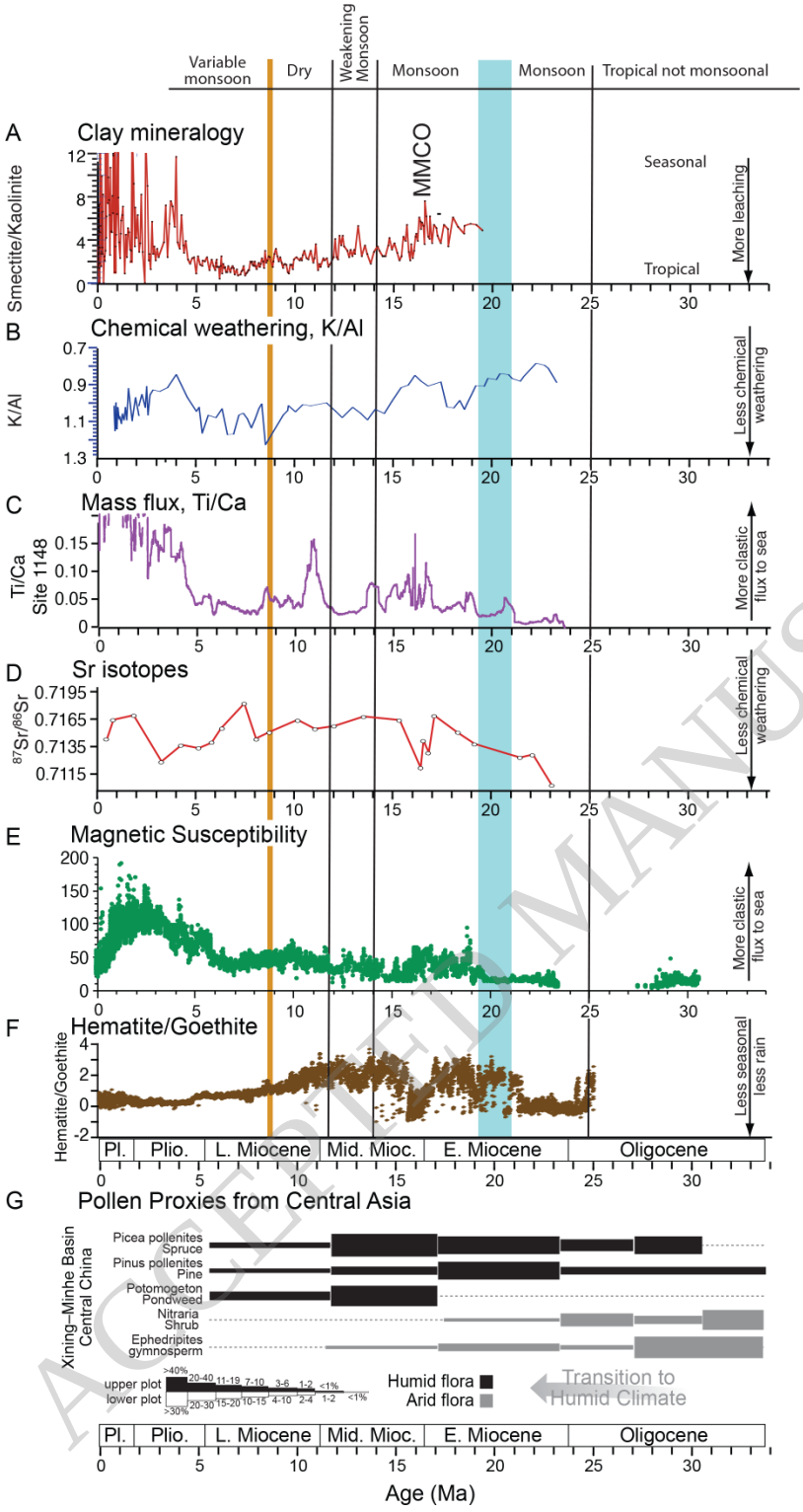

Figure 2

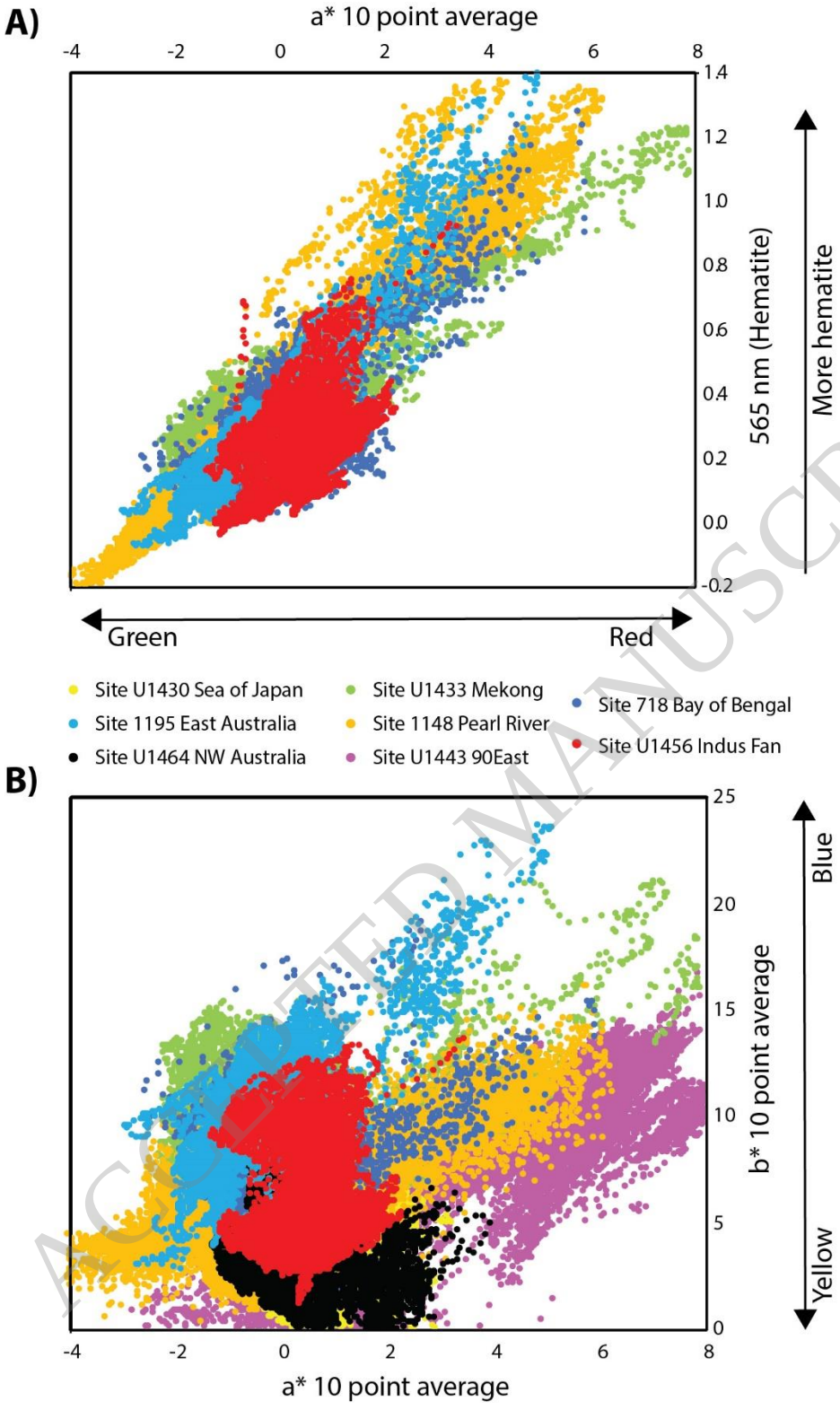

Figure 3

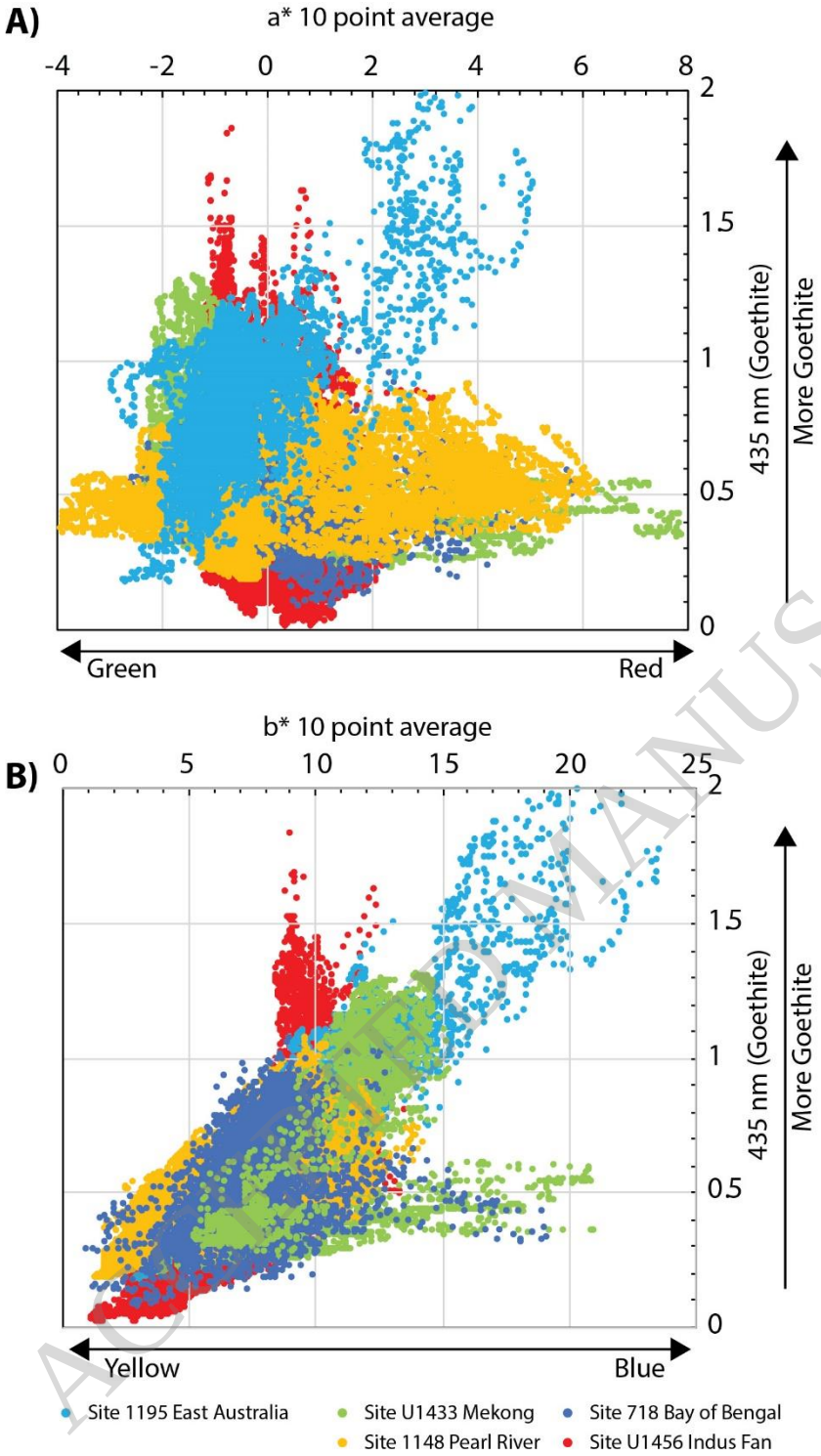

Figure 4

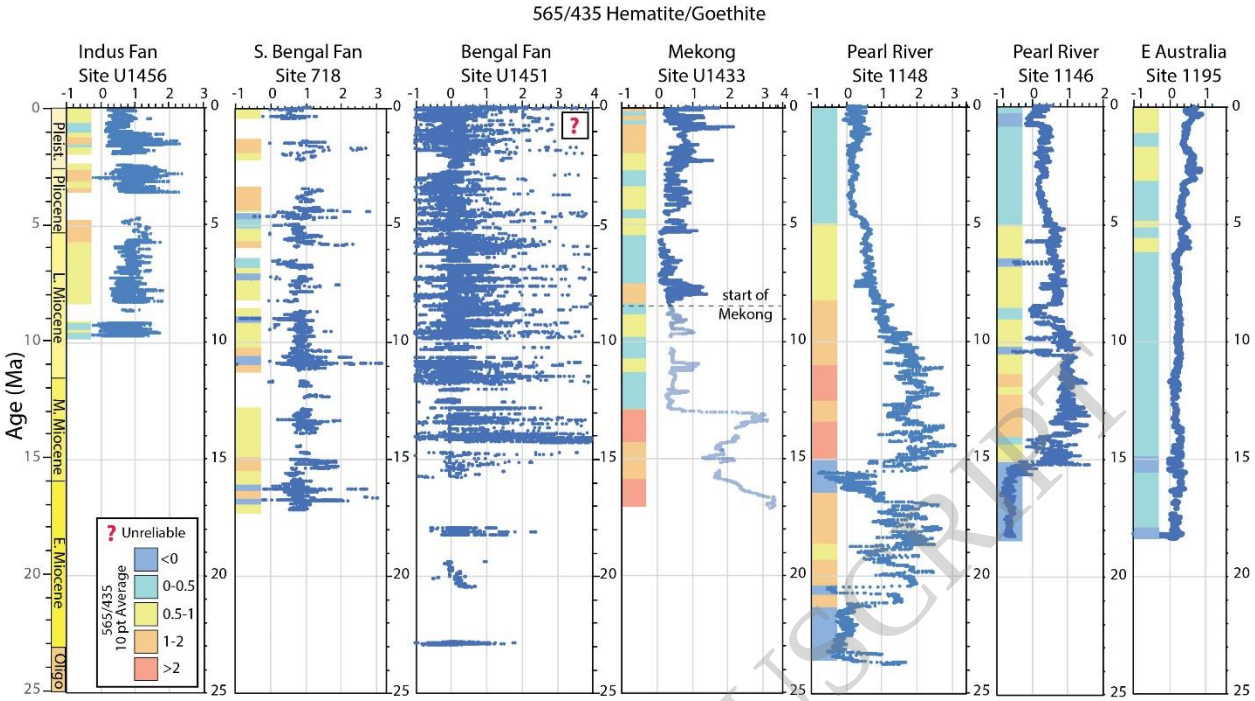

Figure 5

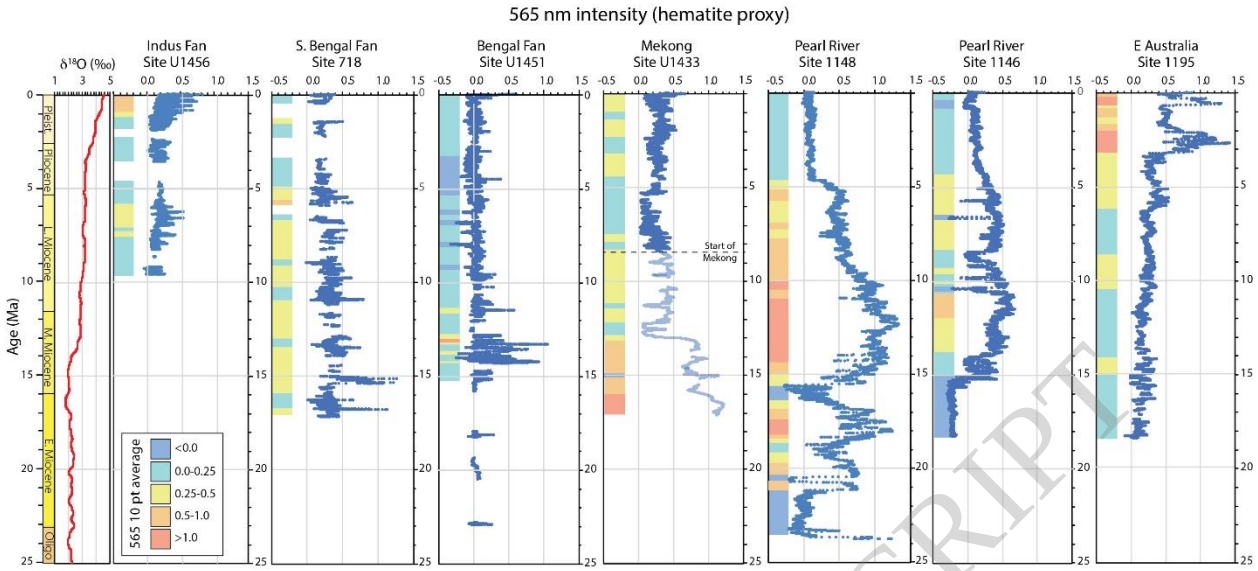

Figure 6

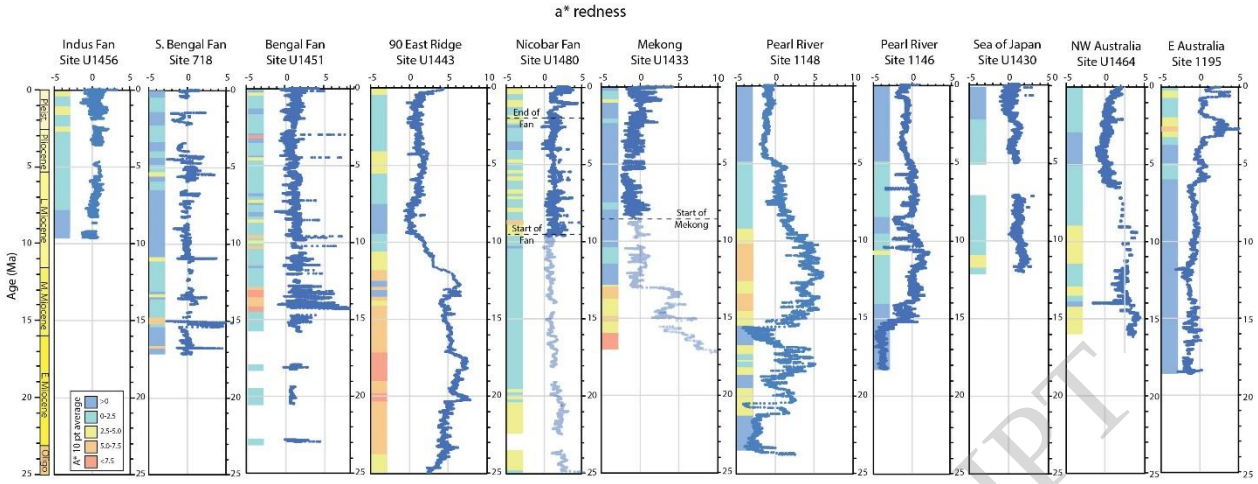

Figure 7
Clift

Figure 7

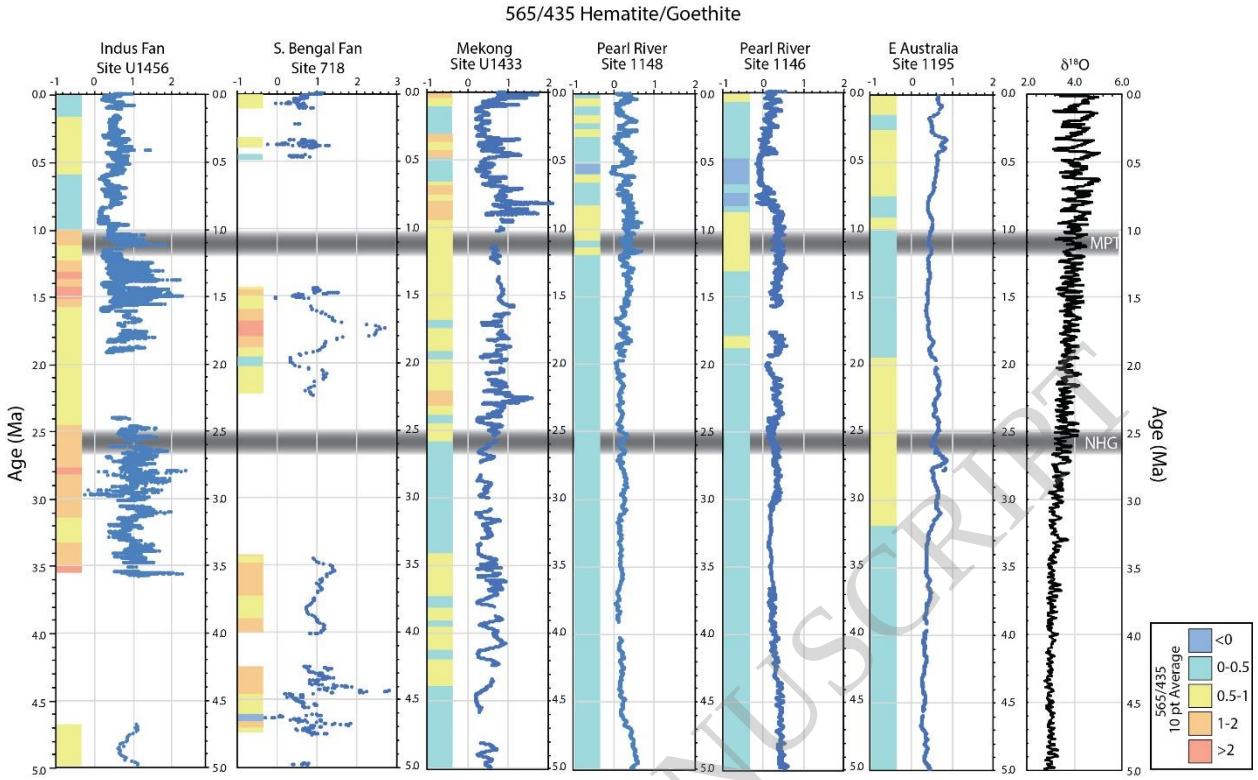

Figure 8

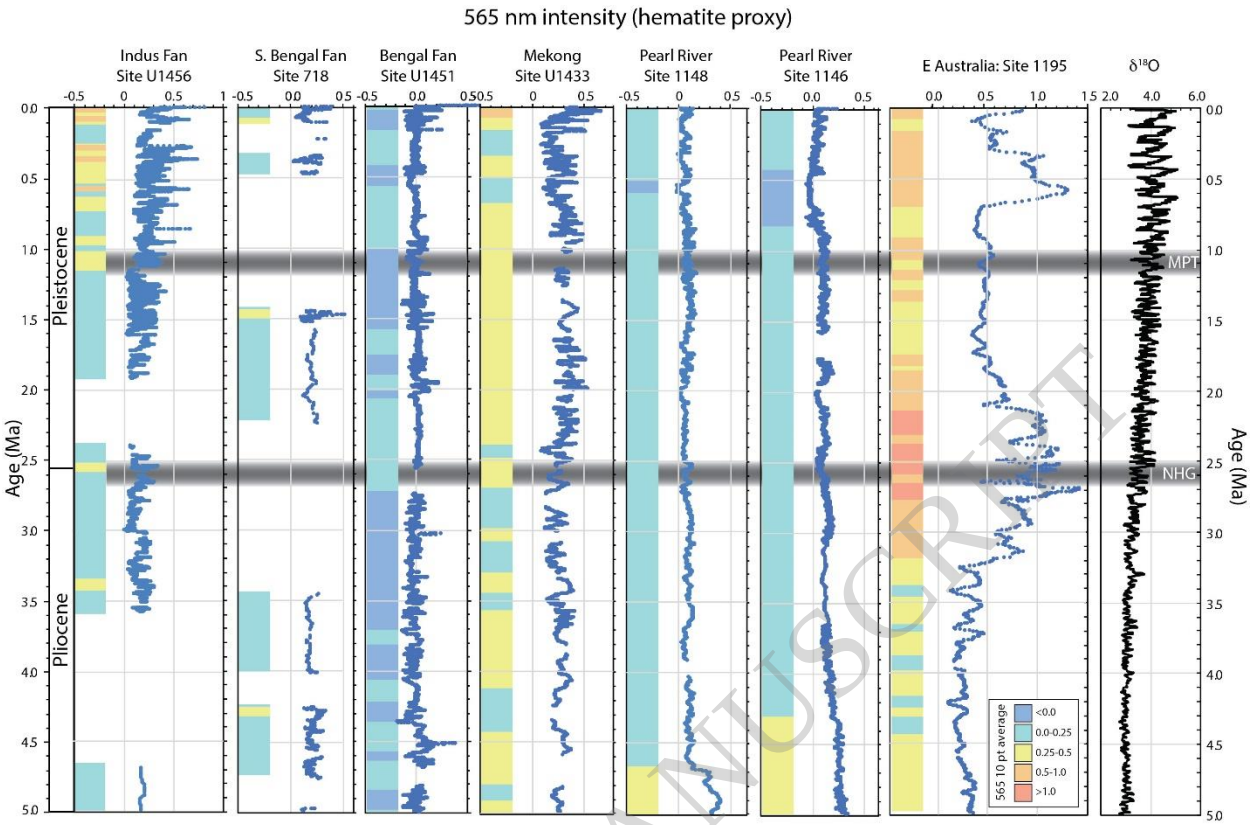

Figure 9

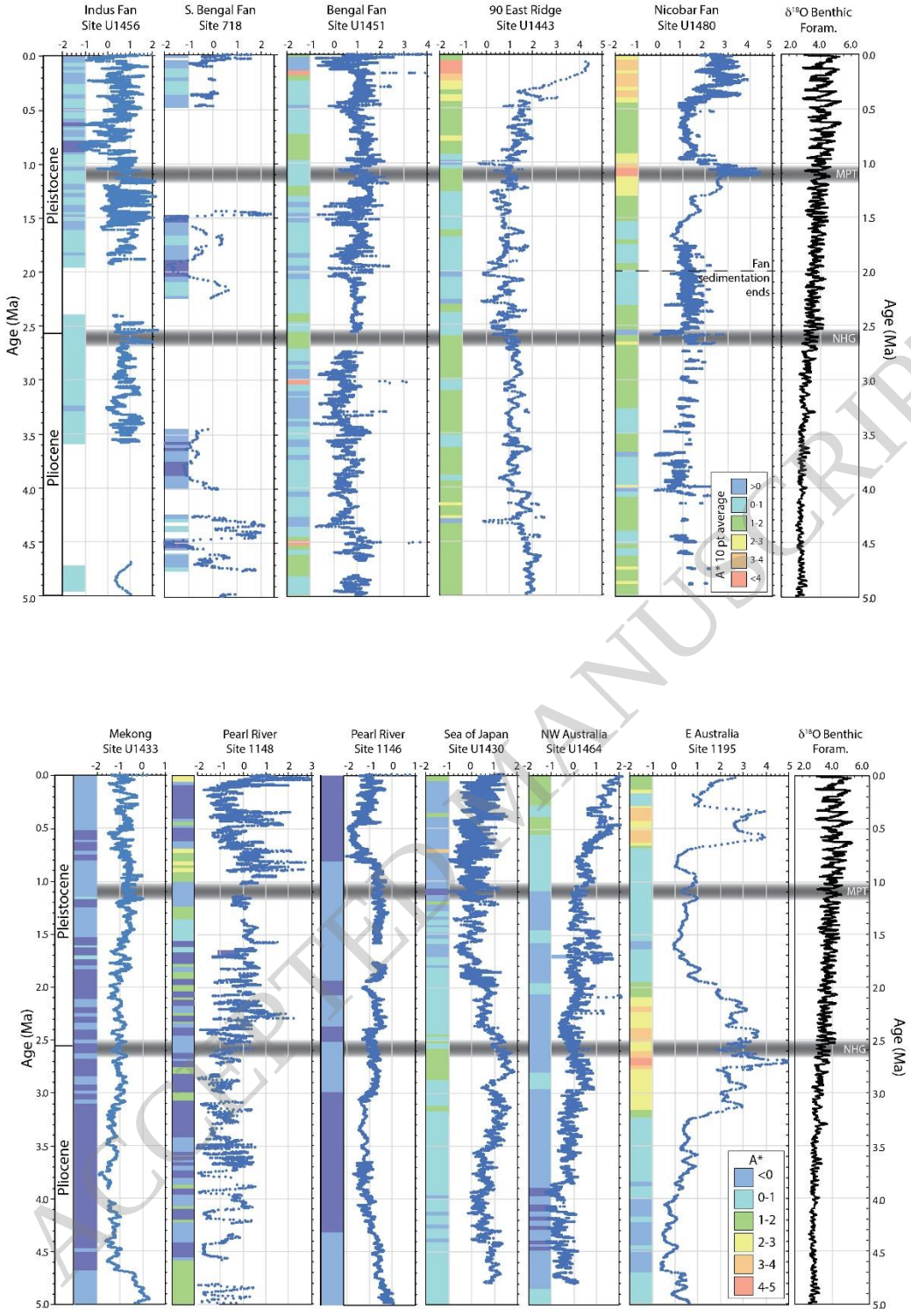

Figure 10

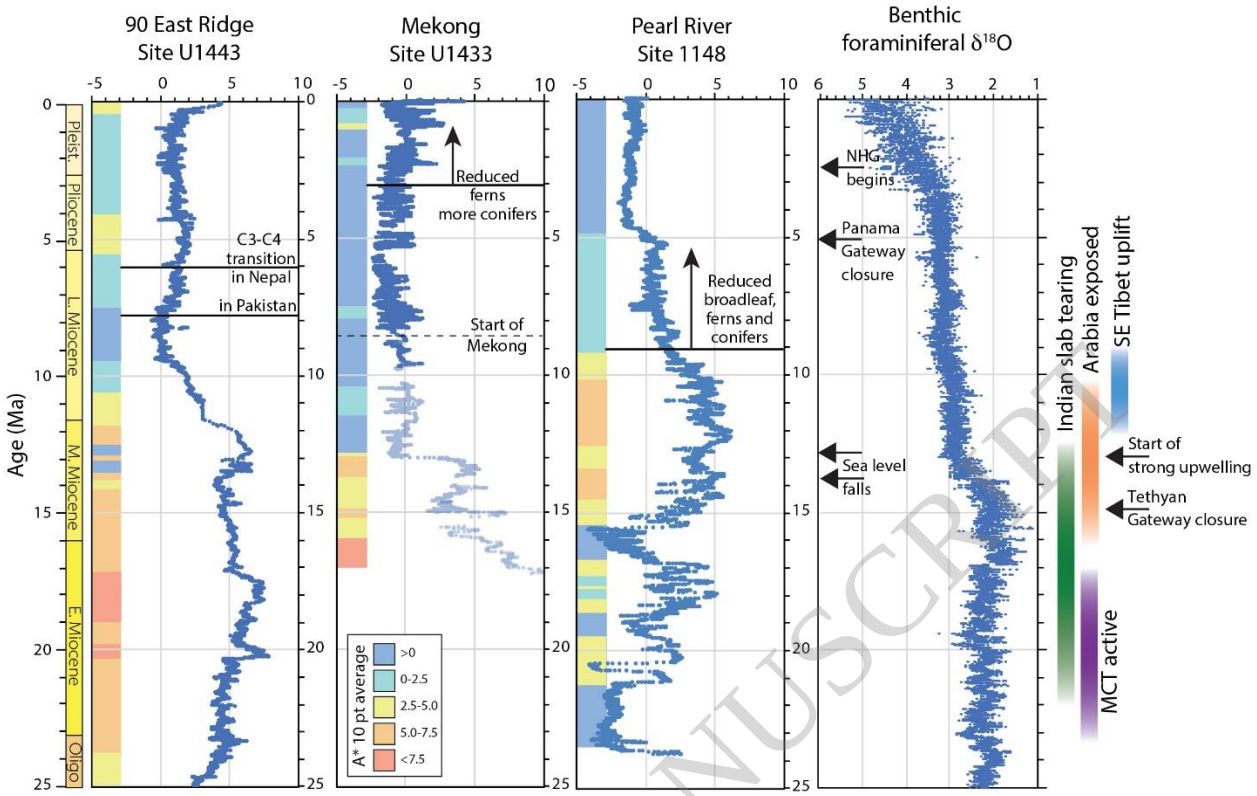

Figure 11

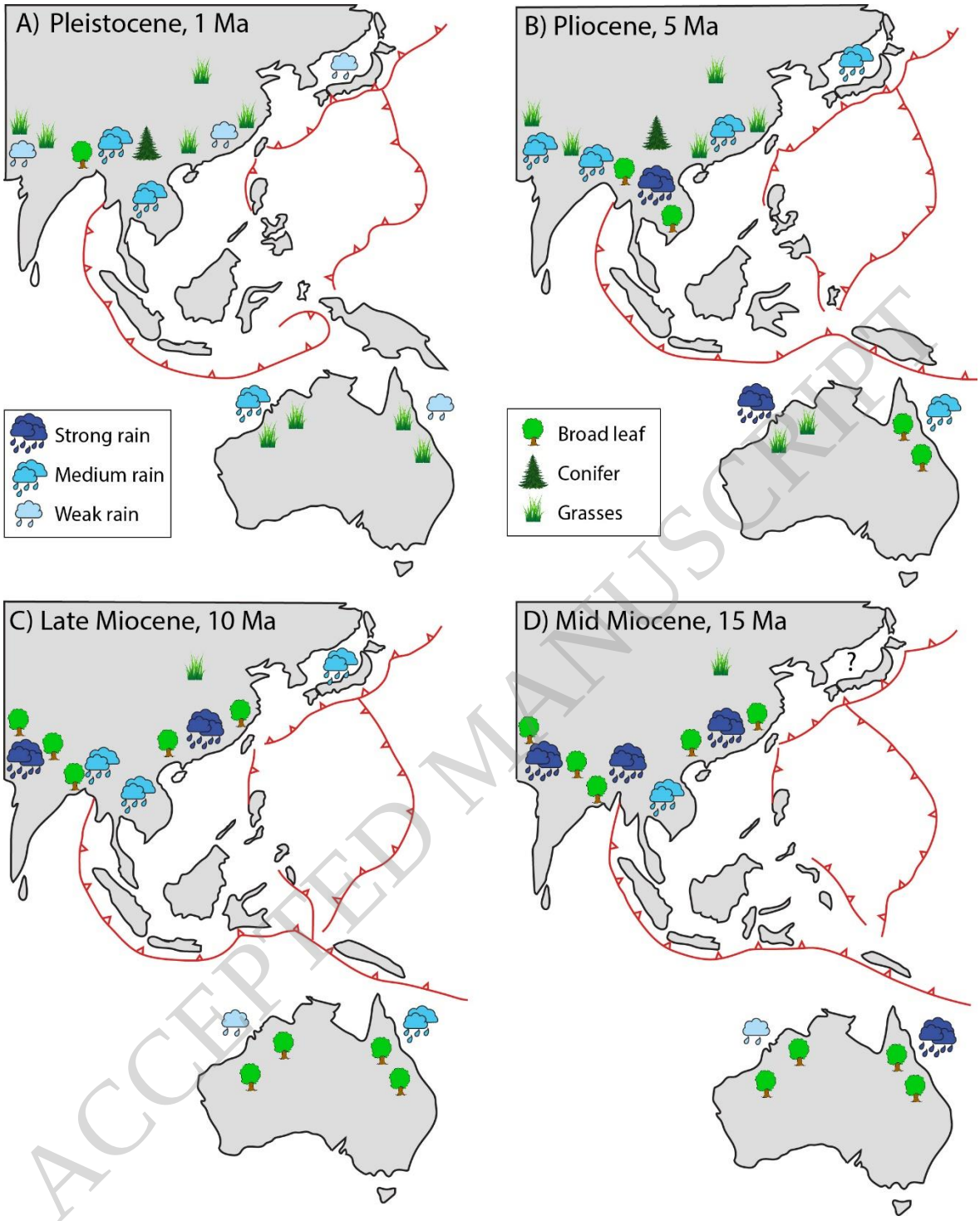

Figure 12

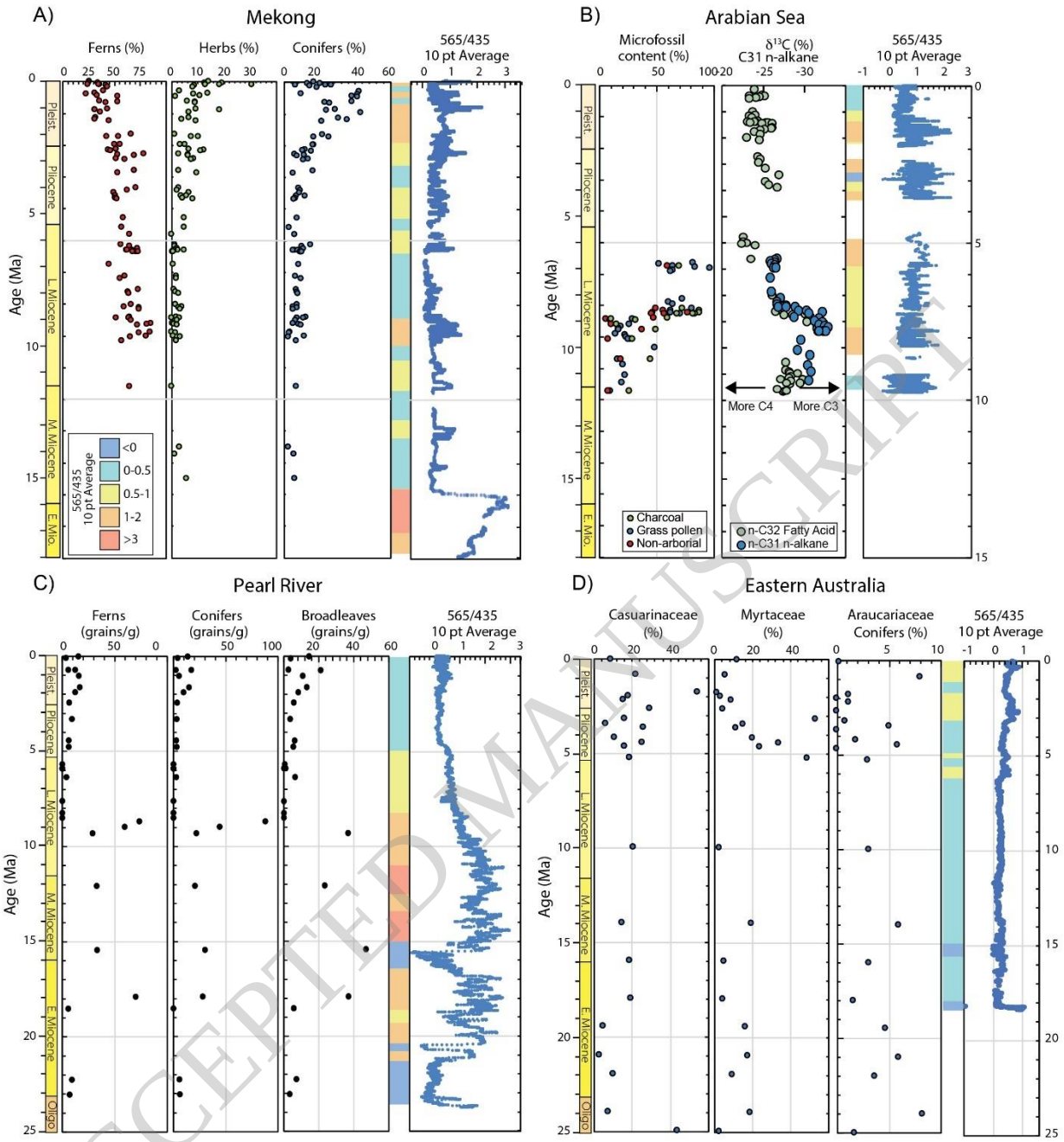

Figure 13